Physics – Uspekhi **69** (3) 282 – 306 (2026)

CONFERENCES AND SYMPOSIA

PACS numbers: **42.55. – f,** 42.60.By, 42.65.Es, 42.65. Hw, 42.68.Wt

PHOTONICS, OPTOELECTRONICS, TERAHERTZ

Nonlinear and linear adaptive optics for laser beam correction *

S.G. Garanin, F.A. Starikov

DOI: https://doi.org/10.3367/UFNe.2025.04.039958

Contents

Abstract. The review is devoted to the research and applications of nonlinear and linear adaptive optics to improve the quality of high power laser beams, including the conditions of its propagation in optically inhomogeneous media. The application of nonlinear adaptive optics is associated with the phase conjugation (wavefront reversal) at stimulated Brillouin scattering in focused beams. The problems of obtaining the high-quality wavefront self-reversal and achieving the diffraction-limited radiation divergence are considered using the example of a two-pass explosive photodissociation iodine laser created at the dawn of quantum electronics and largely determined the energy horizons of its evolution. Linear adaptive optics is associated with an active effect on the radiation phase using methods based both on phase determination and on optimization algorithms. In the case of multichannel lasers, the problem of coherent beam combination is considered, and in the case of a single-channel laser, wavefront control using deformable mirrors is considered. Features of adaptive phase control in the case of continuous and pulsed radiation are discussed.

Keywords: high-power lasers, stimulated Brillouin scattering, phase conjugation, adaptive optics, phase combining of laser beams

S.G. Garanin [(1, a)], **F.A. Starikov** [(1, 2, b)]
[(1)] Russian Federal Nuclear Center–All-Russian Research Institute of Experimental Physics
prosp. Mira 37, 607188 Sarov, Nizhny Novgorod region, Russian Federation
[(2)] Sarov Physical and Technical Institute — branch of National Research Nuclear University MEPhI,
ul. Dukhova 6, 607186 Sarov, Nizhny Novgorod region, Russian Federation
E-mail: [(a)] *SGGaranin@vniief.ru,* [(b)] *FAStarikov@vniief.ru*

Received 29 June 2025
Uspekhi Fizicheskikh Nauk **196** (3) 303 – 329 (2026)
Translated by the authors

1. Introduction

The primary objective of a laser is to ensure the required level of radiation strength and its intensity at the focal spot, which requires increasing the output energy and reducing the angular divergence of the beam. The increase in output energy is limited by physical constraints in the laser's active medium as well as by the radiation loads on the medium and optical components. The angular divergence cannot be less than the diffraction limit λ/D, where λ is the wavelength and D is the beam size, which has an upper limit by physical, technological, and economic reasons. However, as a rule, even at relatively small D values, achieving the diffraction-limited divergence is limited by optical inhomogeneities in the laser's active medium and along the radiation propagation path. Therefore, the crucial task is to create optical systems to reduce beam divergence without significant energy losses. To solve this problem, methods of adaptive optics are used — a scientific field with a wide range of methods and approaches that are difficult to cover in a single review or even a book.

There is some inconsistency in the terminology used in the literature regarding the concept of 'adaptive optics.' Broadly speaking, it refers to the controlled manipulation of an optical system on the radiation field to adapt it to given conditions. It has important applications in science, technology, medicine, and industry, all aimed, in one way or another, at improving the efficiency of wireless energy or information transmission. This review focuses primarily on the adaptive optics for high-power lasers, whose radiation wavefronts are highly aberrated.

The operation of an adaptive optical system can be based on nonlinear or linear effects; therefore, one can speak of

* This review is based on the report presented for the Scientific Session of the Physical Sciences Division of the Russian Academy of Sciences (PSD RAS), on April 2, 2025 (see *Physics–Uspekhi* **69** (3) 281 (2026); *Uspekhi Fizicheskikh Nauk* **196** (3) 302 (2025)).

nonlinear and linear adaptive optics (the latter is often simply called adaptive optics). There are a number of nonlinear effects for beam control [1]. The most suitable of them for high-gain lasers is stimulated Brillouin scattering (SBS), which has wide applications and prospects in optics and photonics (see reviews [2–5]). In the context of high-power lasers, the application of SBS is associated with phase conjugation (PC) [6–9]. At PC realization, the laser beam excites the hypersonic wave in the SBS-active medium and is reflected back from it in such a way that the reflected wave is conjugate to the laser one, i.e., it has the same amplitude-phase structure, propagating in the opposite direction. In the two-pass amplification scheme this allows to automatically compensate for optical inhomogeneities in the laser and the medium during the second pass.

Linear adaptive optics, which originated from the works [10, 11], involves the controlled modification of the wavefront structure of the beam using controllable optical elements [12–15]. It should be noted that linear adaptive optics has many applications unrelated to lasers, for example, in astronomical observations using ground-based telescopes [14, 15]. A number of applications do not involve high-power lasers, for example, in ophthalmology [16], optical communications [17], and biology [18]. Phase control can be achieved through phase shift, phase tip-tilt, and the formation of higher-order phase surfaces. Phase shift control is relevant in the coherent combining of multi-channel radiation. In a single-channel beam, phase tip-tilts can be controlled by the rotating plane mirror, while changes in the wavefront shape is concerned with the use of deformable mirrors [12, 14, 15, 19].

When considering the scope of application for nonlinear and linear adaptive optics in terms of pulse duration, it is easy to see that these approaches are quite complementary. The highest parameters achieved in laser systems worldwide range from continuous-wave operation with power in the tens of kilowatts to femtosecond pulses with petawatt peak power. SBS is the threshold process (in terms of achieving the significant reflection level) [7–9], and the threshold power is in the range of 50–100 kW under typical conditions; therefore, applying SBS in continuous-wave lasers is problematic. SBS can be used for pulse durations shorter than 1 ms, where peak power values significantly exceeding the SBS threshold can be achieved. At the same time, the minimum relaxation time of SBS media is typically more than ~ 1 ns [7–9]. Therefore, it is also impossible to use SBS media in the range shorter than 1 ns, since the medium does not have time to track changes in the laser field. Based on this, the use of SBS is effective for pulsed lasers with pulse durations ranging approximately from 1 ns to 1 ms. It is important to note that the laser field correction under SBS (i.e., PC) occurs in real time.

The application areas for linear adaptive optics lie, accordingly, in the continuous-wave region, where the radiation power is too low to effectively excite SBS, and in the region of pulses shorter than 1 ns, for which the SBS medium is too inert. In the case of short pulses, adaptive optics cannot perform real-time correction; only integral-over-pulse static phase correction is possible here, since the response time of the adaptive system is significantly lower. Therefore, at first, the stability of the laser's operation from pulse to pulse, and at second, the small change in optical inhomogeneities during the pulse duration are of decisive importance here. In continuous-wave lasers, however, real-time phase correction is possible only with relatively slow wavefront distortions (significantly longer than 1 ms), which is owing to the finite response time of the adaptive system components and computer-based mathematical processing.

This review is structured as follows. Section 2 presents the physical and mathematical models of spontaneous emission amplification in laser media and SBS-media, which are used for computational modeling of experiments. Section 3 is devoted to nonlinear adaptive optics. As an example, Section 3.1 describes an explosive photodissociation iodine laser (EPDL). Section 3.2 discusses the PC in the SBS-media using focused beams with a random phase plate and a lenslets array. Section 3.3 presents the results of the study of the EPDL with ultra-high PC quality. Section 3.4 examines the SBS of focused vortex laser beams. Section 4 deals with linear adaptive optics. It examines the coherent combining of multi-channel radiation of continuous-wave fiber lasers (Section 4.1) and the phase control of radiation using flexible adaptive mirrors in the case of continuous-wave and pulsed lasers (Section 4.2).

2. Theory and calculation models

The combination of experiment and theoretical analysis is generally the key to success in physical research. Computational modeling of large-scale laser experiments takes on particular importance when each physical experiment is largely unique and requires lengthy and labor-intensive preparation.

When considering both the processes of stimulated emission at discrete-discrete transitions in excited atoms (i.e., the laser effect) and the processes of stimulated scattering of radiation on density fluctuations in nonlinear media (i.e., SBS), at describing the dynamics of radiation we rely on the system of classical Maxwell equations (see, e.g., [20]):

$$\begin{aligned} &\operatorname{div}\mathbf{B} = 0\,,\\ &\operatorname{div}\mathbf{D} = 0\,,\\ &\operatorname{rot}\mathbf{H} = \left(\frac{4\pi}{c}\right)\sigma\mathbf{E} + \left(\frac{1}{c}\right)\frac{\partial\mathbf{D}}{\partial t}\,,\\ &\operatorname{rot}\mathbf{E} = -\left(\frac{1}{c}\right)\frac{\partial\mathbf{B}}{\partial t}\,, \end{aligned} \tag{1}$$

where $\mathbf{B}$ and $\mathbf{D}$ are the magnetic and electric inductions, $\mathbf{E}$ and $\mathbf{H}$ are the magnetic and electric field strengths, c is the speed of light in vacuum, and σ is the specific electrical conductivity of the medium.

In the case of the laser effect, i.e., when there are radiating atoms and radiation refraction in an isotropic polarizable medium, it is assumed that the term in the third equation of system (1) associated with conductivity phenomenologically accounts for losses arising from absorption caused by all electronic transitions except the laser transition under consideration. In the case of SBS of radiation in the medium, the condition $\sigma = 0$ holds, i.e., the medium is assumed to be transparent to radiation.

The media discussed below are nonmagnetic, and the material equation for electric induction is as follows [20]:

$$\mathbf{D} = \varepsilon\mathbf{E} + 4\pi\mathbf{P}'\,. \tag{2}$$

In the case of the laser effect, ε in (2) represents the dielectric permittivity of the medium, which characterizes its dielectric properties arising from all transitions except the laser transition, while the polarization (dipole moment per unit volume) of the medium associated with the laser transition is separated and denoted by $\mathbf{P}'$. In the case of SBS, however, $\mathbf{P}' = 0$, and the function ε acts as the total dielectric permittivity of the SBS-medium.

Taking into account the transverse nature of light waves and in the quasi-optical approximation (see, for example, [21]), Maxwell's equations (1), together with (2), reduce to a single equation that describes the dynamics of the radiation field in the nonlinear medium:

$$\nabla^2 \mathbf{E} - \frac{1}{c^2}\frac{\partial^2(\varepsilon\mathbf{E})}{\partial t^2} - \frac{4\pi}{c}\frac{\partial(\sigma\mathbf{E})}{\partial t} = \frac{4\pi}{c^2}\frac{\partial^2 \mathbf{P}'}{\partial t^2}\,. \tag{3}$$

The further adaptation of equation (3) for cases involving laser amplification and SBS of radiation differs in nature.

2.1 Laser amplification

Since, in the case of laser amplification, the medium parameters σ and ε vary more slowly than the electric field E, they can be factored out from under the derivative sign in (3). Let us define the refractive index of the medium $n = \varepsilon^{1/2}$, which is associated with all transitions except the laser transition under consideration. Let us introduce the absorption coefficient $\kappa = 4\pi\sigma/cn$ such that, in the absence of polarization of the medium, the flux density of the plane wave propagating along the z axis decreases as $\exp(-\kappa z)$. Then (3) takes the form of the wave equation with damping and the nonhomogeneous right-hand side:

$$\nabla^2 \mathbf{E} - \frac{n^2}{c^2}\frac{\partial^2 \mathbf{E}}{\partial t^2} - \kappa\frac{n}{c}\frac{\partial \mathbf{E}}{\partial t} = \frac{4\pi}{c^2}\frac{\partial^2 \mathbf{P}'}{\partial t^2}\,. \tag{4}$$

To describe many coherent resonant interactions, only two laser levels are relevant, even though the laser medium has the complex, branched energy structure. Therefore, the two-level approximation is often good first approximation when describing the medium's interaction with radiation [22]. For polarization $\mathbf{P}'$ and population inversion $\Delta N = N_u - N_l$, the following equations hold for an isotropic two-level medium [20, 22]:

$$\frac{\partial^2 \mathbf{P}'}{\partial t^2} + \frac{2}{\tau_2}\frac{\partial \mathbf{P}'}{\partial t} + \omega_0^2 \mathbf{P}' = -\frac{2\omega_0}{3\hbar}\left|\mathbf{d}_{ul}\right|^2 \Delta N\,\mathbf{E}\,, \tag{5}$$

$$\frac{\partial \Delta N}{\partial t} + \frac{\Delta N - \Delta N_0}{\tau_1} = \frac{2}{\hbar\omega_0}\,\mathbf{E}\,\frac{\partial \mathbf{P}'}{\partial t}\,, \tag{6}$$

where τ_1 and τ_2 are the longitudinal and transverse relaxation times, respectively, ω_0 is the frequency of the $l-u$ laser transition, $\mathbf{d}_{ul}$ is the matrix element of the dipole moment operator for the $u-l$ transition, N_u and N_l are the population densities of the upper and lower laser levels, ΔN_0 is the population inversion in the absence of radiation. In (5) and (6), the condition $n^2 \cong 1$ is used, which is characteristic of gaseous laser media.

The transverse relaxation time τ_2 is the characteristic time of the exponential decay of the dipole, reflecting both radiative and collisional processes that lead to dephasing and broadening the Lorentzian profile of the spectral line. Equation (6) defines the energy balance in the system and relates the change in stored energy to the change in polarization and the field. The distribution of ΔN_0 depends on the pumping conditions of the working medium. The longitudinal relaxation time τ_1 characterizes the rate of energy decay and depends on the rates of the elementary processes in the medium.

The simplification of the system (4)–(6) consists in adopting the quasi-optical approximation, in which laser radiation is treated as the "quasi-planar and quasi-monochromatic wave" [23]. It should be noted that laser radiation is highly directional. In the case of the laser generator, this is the consequence of the elongation of the laser medium and the presence of an open resonator (in the mirrorless laser, beam formation is provided solely by the elongation of the medium). In the case of the laser amplifier, the beam with low divergence is fed into its input.

Suppose that the polarization (the orientation of the field strength vector) of the radiation does not change significantly as it propagates, so that the scalar wave equation can be used instead of the vector equation (4). This approach accounts for the amplification of both the radiation incoming from outside and the spontaneous noise generated within the medium itself. This fact, as well as the presence of reflecting mirrors, requires us to consider the amplification of two waves propagating in mutually opposite directions. The amplitude of such 'quasi-plane waves' varies slowly along the propagation axis z, and the dimensions of the laser beam in the transverse plane (x, y) are much smaller than the characteristic dimensions along the z-axis. We will label the quantities corresponding to the opposite waves with the indices '+' and '−'. Then, we seek the solution of equation (4) in the form of two waves propagating in opposite directions along the z-axis:

$$\mathbf{E}(\mathbf{R}, t) = \mathbf{i}_e \mathrm{Re}\left[A_+(\mathbf{r}, z, t)\,\exp(-\mathrm{i}kz + \mathrm{i}\omega t) + A_-(\mathbf{r}, z, t)\,\exp(+\mathrm{i}kz + \mathrm{i}\omega t)\right]. \tag{7}$$

Here, the complex functions A_+ and A_- represent the slowly varying amplitudes of the laser radiation fields, and $\mathbf{r} = \mathbf{i}x + \mathbf{j}y$ is the transverse radius vector. The quantity ω in (7) is the characteristic frequency of radiation with the narrow spectral line, $k = n_0\omega/c$ is the characteristic wave number, and n_0 is the average refractive index. Thus, we assume that the wave number k varies in the medium much more slowly than the amplitudes of the fields A_+ and A_-, and the characteristic time of variation of A_+ and A_- significantly exceeds the oscillation period.

Similarly, it is assumed that the polarization $\mathbf{P}'$ associated with the transition under consideration varies in the same way as the electric field $\mathbf{E}$:

$$\mathbf{P}'(\mathbf{R}, t) = \mathbf{i}_p\,\mathrm{Re}\left[p_+(\mathbf{r}, z, t)\,\exp(-\mathrm{i}kz + \mathrm{i}\omega t) + p_-(\mathbf{r}, z, t)\,\exp(+\mathrm{i}kz + \mathrm{i}\omega t)\right]. \tag{8}$$

where p_+ and p_- are complex functions of coordinates and time that vary slowly compared to the exponential multiplier.

Let us substitute (7) and (8) into (4)–(6) and assume that the characteristic frequency ω of the radiation is close to the transition frequency ω_0. Since $\varepsilon \cong 1$, it is appropriate to take the inhomogeneity of ε into account only in the term responsible for refraction. Changes in the population inversion ΔN over distances of the order of the wavelength and over times of the order of the radiation oscillation period are negligibly small. Taking these assumptions into account, we

obtain the system of reduced equations from (4)–(6):

$$\left[\pm\frac{\partial}{\partial z}+\frac{1}{c}\frac{\partial}{\partial t}+\frac{\mathrm{i}}{2k}\nabla_{\perp}^{2}+\frac{\mathrm{i}k}{2}(\varepsilon-1)+\frac{\kappa}{2}\right]A_{\pm}=\frac{k}{2\mathrm{i}}p_{\pm}, \quad (9)$$

$$\left[\frac{\partial}{\partial t}+\frac{1}{\tau_2}\right]p_{\pm}=\frac{\mathrm{i}\alpha}{k\tau_2}A_{\pm}+S_{\pm}, \quad (10)$$

$$\frac{\partial\Delta N}{\partial t}+\frac{\Delta N-\Delta N_0}{\tau_1}=-\frac{2}{\hbar c}\,\mathrm{Im}\,(A_{+}^{*}p_{+}+A_{-}^{*}p_{-}), \quad (11)$$

where $\nabla_{\perp}^{2}$ is the Laplacian in the transverse coordinates.

We take into account the amplification of intrinsic spontaneous radiation along with external incident radiation, the level of which is determined by the boundary conditions. It should be noted that in the semi-classical approach, it is impossible to strictly account for spontaneous emission, which, according to quantum electrodynamics, arises from vacuum fluctuations. Nevertheless, the description of spontaneous radiation is possible in an improved semi-classical approach, supplemented by the specific logic of vacuum fluctuations [24]. It has been shown [25] that the description of amplified spontaneous emission is determined by the system of equations for the field and polarization operators, which is formally identical to the semi-classical system of equations (for the single emission flux) with an additional Langevin fluctuation force S on the right-hand side of the equation for the medium polarization. In our case of two radiation fluxes, appropriate, statistically independent and delta-correlated terms S_{+} and S_{-} are phenomenologically added to both equations for p_{+} and p_{-} in (10):

$$\langle S_{\pm}(\mathbf{r}_1,z_1,t_1)\,S_{\pm}^{*}(\mathbf{r}_2,z_2,t_2)\rangle=\frac{2}{\tau_2}\,16\pi c\,\frac{|\mathbf{d}_{ul}|^2}{3}\,N_u\delta^{(2)}(\mathbf{r}_1-\mathbf{r}_2)\times\delta(z_1-z_2)\delta(t_1-t_2). \quad (12)$$

Equation (10) also employs the condition $\Delta\omega=\omega_0-\omega=0$, i.e., the carrier frequency of the radiation is chosen to be equal to the frequency of the laser transition, which is assumed to be constant throughout the entire ensemble of emitters; thus, the line-broadening mechanism is homogeneous in nature. If Lamb shifts are neglected, the additional inhomogeneous (Doppler) line broadening can be accounted for within the framework of the Lorentzian contour. Otherwise, if the Doppler broadening is significant, it is necessary to solve the system of equations for p_{+} and p_{-} in (10), each of which is characterized by its own frequency detuning $\Delta\omega$. In this case, the right-hand side of the equations for the fields A_{+} and A_{-} in (11) will contain the sum of the quantities p_{+} and p_{-} with different $\Delta\omega$, and each of these quantities will be included in the sum with the weight corresponding to the inhomogeneous (Gaussian) line profile at a given temperature. We do not use the multi-group approach, since the main focus is on examining spatial effects in radiation dynamics, and in the case of EPDL, the Doppler line broadening is significantly smaller than the Lorentzian one.

Furthermore, in (10), the radiation gain coefficient for the laser transition is introduced in units of inverse length as $\alpha=\sigma\Delta N$, where $\sigma=4\pi k\tau_2|\mathbf{d}_{ul}|^2/3\hbar$ is the cross section of the radiative transition at $\omega=\omega_0$ [26]. Furthermore, using the relationship between the Poynting vector and the field intensity, for the convenience of normalizing the field amplitudes A_{+}, A_{-} are multiplied by $\sqrt{c/8\pi}$, so that the radiation energy flux densities (in W cm^{-2}) are equal to $J_{\pm}=|A_{\pm}|^2$. The amplitudes of the polarizations p_{+}, p_{-} are multiplied by the value $\sqrt{2\pi c}$.

The system of equations (9)–(11) is based on an approach traditionally referred to in the English-language literature as the Maxwell–Bloch approach [22]. The parabolic equation (9), together with equations (10) and (11), form the closed system of equations describing the interaction of laser radiation with the two-level quantum medium, taking into account the transient processes associated with the finiteness of the times τ_1 and τ_2.

To solve the system of equations (9)–(11), information is needed about the spatiotemporal distribution of the unrelaxed population inversion in the absence of radiation ΔN_0. This quantity is determined by the pumping conditions and the characteristics of the laser medium's energy structure, and it is not easy to estimate it under practical conditions. In practice, under the conditions of the specific multi-level medium, instead of single equation (11), one must consider a system of equations describing the population dynamics of all significant energy levels, the kinetics of which can affect the population inversion in the laser transition. In the case of EPDL, this includes the kinetics of photochemical processes, chemical reactions, and radiative and nonradiative electronic transitions. There are usually quite a few such levels, and their number is chosen depending on the desired accuracy. One must also take into account additional factors that degrade the accuracy of the calculations (accuracy of reaction rates, spectroscopic constants, etc.). In the general case, the system of local balanced kinetic equations for M energy levels takes the form:

$$\frac{\mathrm{d}N_i}{\mathrm{d}t}=D_i+\sum_j K_{ji}N_j-(\delta_{iu}-\delta_{il})\frac{1}{\hbar c}\,\mathrm{Im}\,[A_{+}^{*}p_{+}+A_{-}^{*}p_{-}],\quad i=1,\ldots,u,\ldots,l,\ldots,M. \quad (13)$$

Here K_{ji} is the relaxation matrix of the rates of various elementary processes; D_i is the electron flux into state i from the continuum and states not accounted for by the relaxation matrix. The population inversion is found from the relation $\Delta N=N_u-g_uN_l/g_l$, assuming possible degeneracy of the laser levels (g_u and g_l are the statistical weights of the upper and lower laser levels).

An analytical solution to equations (9)–(11) is possible in the simplest cases, but their practical value is limited, since under actual conditions, the distributions of environmental parameters exhibit complex spatiotemporal characteristics. In this regard, the development of appropriate numerical models appears to be of particular relevance [27, 28]. The coordinated and simultaneous solution of the system of equations (9) and (10) with population kinetics is often complicated by the fact that the latter model cannot initially be reduced to the single equation for inversion (11), but instead requires solving the system of kinetic equations (13), of which there may be quite a large number. This can lead to unrealistically long computation times. Therefore, in many practical situations, the system of equations (13) is first solved separately, neglecting stimulated emission in the laser transition.

Generally speaking, there are three possible approaches to determining the medium parameters. First, experimental data can be used for this purpose, provided it is available in sufficient detail. Second, model profiles of medium parameters can be employed, based on prior assumptions and theoretical estimates. This approach is suitable for establish-

ing general patterns of radiation dynamics but is insufficient for modeling the specific systems. Third, special models and programs for thermodynamics, hydrodynamics, and multilevel population kinetics are developed — this is precisely the case where determining the medium parameters becomes the separate problem [29]. In any case, the result of solving the kinetic problem is the spatiotemporal distribution of ε, κ and the gain coefficient at the laser transition in the weak-signal approximation (i.e., in the absence of stimulated emission). The formula for the latter is given by $\alpha_0 = \sigma\Delta N_{r0}$, where the quantity ΔN_{r0} differs from ΔN_0 in that it takes into account the relaxation of the inversion.

In the subsequent analysis of the dynamics of laser radiation, the obtained distributions ε and κ are used in the integration of (9). The correct account of gain in (10) covers two cases. In the first case, linear gain is considered. The linear amplification approximation applies when the intensity of the laser radiation in the medium is significantly less than the saturation intensity $J_{\text{sat}} = \hbar\omega k^2/(2\pi\tau_1\tau_2 A_{ul})$, where A_{ul} is the probability of the spontaneous radiative transition between the upper u and lower l laser levels. In this case, equations (9) and (10) are integrated with the given distribution of the weak signal gain coefficient α_0, obtained after solving the system (13).

The second case occurs when the linear amplification condition is not satisfied and the amplified radiation fluxes are significant; in this case, the consistent solution to equations (9)–(11) is required. The value of ΔN_0 is unknown, but the solution of the complete system of kinetic equations (13) is available — the spatiotemporal distribution of population inversion ΔN_{r0}. Since this quantity, obtained also in the absence of radiation, already accounts for the relaxation of the inversion, an equation for the inversion can be derived from (13) in the form:

$$\frac{\partial\Delta N}{\partial t} = \frac{\partial\Delta N_{r0}}{\partial t} - \frac{1+g_u/g_l}{\hbar c}\,\mathrm{Im}\,(A_+^* p_+ + A_-^* p_-)\,. \qquad (14)$$

Next, in the process of solving equation (14), the gain coefficient $\alpha = \sigma\Delta N$ is determined by simultaneously solving equations (9) and (10).

The initial conditions for the polarizations and both spontaneous sources are given by [27, 28]:

$$\langle p_{\pm0}(\mathbf{r}_1, z_1) p_{\pm0}^*(\mathbf{r}_2, z_2)\rangle = \left(\frac{4j_s}{k^2}\right) F_s(\mathbf{r}_1 - \mathbf{r}_2)\delta(z_1 - z_2)\,,$$

$$\langle S_\pm(\mathbf{r}_1, z_1, t_1) S_\pm^*(\mathbf{r}_2, z_2, t_2)\rangle = \left(\frac{2}{\tau_2}\right)\langle p_{\pm0}(\mathbf{r}_1, z_1) p_{\pm0}^*(\mathbf{r}_2, z_2)\rangle \times \delta(t_1 - t_2)\,,$$

where $F_s(\mathbf{r}_1 - \mathbf{r}_2)$ is the dimensionless transverse correlation function, which yields the spontaneous emission brightness of one, j_s is the spontaneous emission power per unit volume of the medium per solid angle (measured in W cm^{-3} sr^{-1}), which equals to $j_s = \hbar\omega A_{ul} N_u/(4\pi) = \hbar\omega^3 f_{ul} N_u/(2\pi mc^3)$, where A_{ul} and f_{ul} are the probability and oscillator strength of the spontaneous transition $u \to l$ [30].

If we neglect transient processes, where the quantities p_+ and p_- are simply expressed in terms of field amplitudes, the system (9)–(11) reduces to equations (9) and (11) or (14).

2.2 Stimulated Brillouin scattering

SBS process occurs when a medium is exposed to intense laser radiation and is characterized by the interaction between the medium and the field (via scattering) and between the field and the medium (via the electrostriction effect). Naturally, the medium cannot keep up with changes in the field of laser wave propagating at the speed of light. The SBS process starts from the stage of the spontaneous scattering of laser radiation on thermal fluctuations in the medium, which propagate at acoustic speeds and decay. Due to the Doppler effect, the wave reflected from the density inhomogeneity undergoes the frequency shift. The laser wave and the scattered wave form an interference pattern of intensity in the medium, which propagates more slowly, at the acoustic speed. In turn, through the mechanism of electrostriction, it begins not only to sustain the decaying fluctuations of the medium but also to oscillate the acoustic wave, provided the intensity of the laser pumping is sufficiently high. The scattering of radiation on the acoustic wave takes the form of parametric amplification [31]. Scattering is possible at any angle, but the greatest amplification is observed in the extended channel of the laser beam, which forms the gain region.

In the case of SBS, the medium is assumed to be transparent to radiation, i.e., $\sigma = 0$ (this refers to nonresonant absorption not associated with energy transfer from the incident wave to the scattered wave). Furthermore, $\mathbf{P}' = 0$ in (3), and the function ε plays the role of the total dielectric permittivity of the SBS medium, $\varepsilon = n^2$, where n is the refractive index. In this case, the acoustic vibrations of the medium follow the oscillations of the total field $\mathbf{E}$, so ε in (3) cannot be taken out from under the derivative sign. As a result, (3) takes the form:

$$\nabla^2\mathbf{E} - \frac{1}{c^2}\frac{\partial^2(\varepsilon\mathbf{E})}{\partial t^2} = 0\,. \qquad (15)$$

We assume that the various nonlinear processes in the medium evolve independently of one another, and that the nonlinear response of the medium is sufficiently weak. Let us introduce small deviations in density ρ, pressure p, and permittivity — from their equilibrium values:

$$\rho = \rho_0 + \rho'\,, \qquad p = p_0 + p'\,, \qquad \varepsilon = \varepsilon_0 + \varepsilon' \qquad (16)$$

provided that the conditions $\rho' \ll \rho_0$, $p' \ll p_0$, $\varepsilon' \ll \varepsilon_0$ are satisfied. The equilibrium velocity of the medium is zero: $\mathbf{v} = \mathbf{v}'$.

In the expansion of the dielectric permittivity deviation in terms of pressure fluctuations, we will limited to the first term: $\varepsilon' = p'(\partial\varepsilon/\partial p)_s$, or, using standard notation

$$\varepsilon' = \left(\frac{\partial\varepsilon}{\partial\rho}\right)_s\left(\frac{\partial\rho}{\partial p}\right)_s p' = \rho\left(\frac{\partial\varepsilon}{\partial\rho}\right)_s\frac{p'}{\rho(\partial p/\partial\rho)_s} = Y\beta_s p'\,,$$

where $Y = \rho(\partial\varepsilon/\partial\rho)_s$ is the nonlinear coupling parameter; $\beta_s = 1/(\rho v_s^2)$ is the compressibility of the medium; $v_s^2 = (\partial p/\partial\rho)_s$, v_s and vs is the adiabatic speed of sound. There is the linear relationship between density and pressure: $p' = (\partial p/\partial\rho)_s\rho' = v_s^2\rho'$.

If we assume that the average dielectric properties of undisturbed medium change sufficiently slowly during the period of the field oscillations, then (15), taking (16) into account, can be rewritten as:

$$\frac{n_0^2}{c^2}\frac{\partial^2\mathbf{E}}{\partial t^2} - \nabla^2\mathbf{E} = -\frac{Y\beta_s}{c^2}\frac{\partial^2(p'\mathbf{E})}{\partial t^2}\,, \qquad (17)$$

where $n_0^2 = \varepsilon_0$, n_0 is the slowly varying refractive index of the medium undisturbed by sound.

To describe the SBS process, it is necessary to simultaneously solve the equation of electromagnetic field propagation in the dielectric (17) and the equations describing the state of the medium taking viscosity into account. This is fundamental, since the magnitude of viscous damping determines the amplitude of the sound wave and, consequently, the efficiency of resonant scattering. These latter equations are reduced to the wave equation for pressure variation [31]:

$$\frac{\partial^2 p'}{\partial t^2} - \nabla^2\left(v_s^2 p' + \Gamma\,\frac{\partial p'}{\partial t} - \frac{Y}{8\pi\rho\beta_s}\,\mathbf{E}^2\right) = 0\,. \tag{18}$$

In (18), the damping constant $\Gamma = (4\eta/3 + \eta')/\rho_0$ is introduced to characterize the damping of pressure (density) inhomogeneities, where η and η' are the shear and bulk viscosities, respectively. For a gaseous medium, more accurate expression for Γ is obtained by accounting for heat transfer, when the process is no longer strictly adiabatic: $\Gamma = [4\eta/3 + \eta' + \Lambda(1/c_V - 1/c_P)]/\rho_0$, where Λ is the thermal conductivity of the medium, and c_P and c_V are the specific heat capacities at constant pressure and volume. The inhomogeneous term with $\mathbf{E}^2$ in (18) reflects the action of electrostrictive forces exerted by the field on the SBS medium.

The system (17), (18), like the system (4)–(6), serves as the basis for subsequent reduction of the equations, similar to Section 2.2. The solutions to (17) and (18) are represented as 'quasi-plane' waves with slowly varying amplitudes.

The scattered radiation has the frequency shift relative to the incident laser radiation with frequency ω_L [31]

$$\Omega = \pm 2n_0\,\frac{v_s}{c}\,\omega_L \sin\frac{\theta}{2}\,, \tag{19}$$

where θ is the scattering angle. In backscattering ($\theta = \pi$), the frequency is at its maximum; an estimate for the optical wavelength range shows that Ω lies in the hypersonic range (1–100) GHz. The Stokes component has the negative frequency shift, and the anti-Stokes component is excluded from consideration due to the ineffectiveness of its stimulated scattering [31]. The choice of active medium geometry in SBS tasks (elongated in the direction of the propagation of the pump laser beam) ensures that the Stokes component is predominantly reflected almost strictly backward. Therefore, in the scalar approximation, the light field can be represented as the sum of two waves traveling along the z-axis toward each other:

$$\mathbf{E} = \mathbf{i}_e \mathrm{Re}\big[A_L \exp\big(\mathrm{i}(\omega_L t - k_L z)\big) + A_S \exp\big(\mathrm{i}(\omega_S t + k_S z)\big)\big], \tag{20}$$

where the subscript 'L' refers to the laser wave, and the subscript 'S' refers to the reflected Stokes wave.

The frequency of the hypersonic wave is equal to the Stokes shift: $\omega_L = \omega_S + \Omega$. In the case of SBS, Bragg's condition holds for the corresponding wave vectors: $\mathbf{k}_L = \mathbf{k}_S + \mathbf{q}$. In accordance with these conditions, the resonant hypersonic wave corresponding to the light wave expression (20) takes the form:

$$p' = \mathrm{Re}\, p \exp\big(\mathrm{i}(\Omega t - qz)\big)\,, \tag{21}$$

where Ω and $q \approx 2k_L$ are the frequency and wave number of the hypersonic wave, and p is the complex pressure amplitude of hypersonic wave.

We will assume that the amplitudes of the laser and Stokes fields, A_L and A_S, and the hypersonic field, p, vary smoothly over distances of the order of the wavelengths of light and hypersonic waves, which are of the same order of magnitude. In this case, the values of A_L, A_S, and p will always vary slowly against the background of light field oscillations, but not always on the scale of hypersonic oscillations, since the wavelengths of light and hypersonic waves are close whereas Ω is significantly smaller than ω_L.

Substituting (20), (21) into the system (17), (18), grouping the expressions by corresponding exponents and neglecting the second derivatives of the slow amplitudes and the rapidly oscillating terms, we obtain the following system of reduced equations [32–35]:

$$\frac{n_0}{c}\,\frac{\partial A_L}{\partial t} + \frac{\partial A_L}{\partial z} + \frac{\mathrm{i}}{2k_L}\nabla_\perp^2 A_L + \frac{\mathrm{i}k}{2}\left(\frac{n^2}{n_0^2} - 1\right)A_L = -\frac{\mathrm{i}}{2}\,pA_S, \tag{22}$$

$$\frac{n_0}{c}\,\frac{\partial A_S}{\partial t} + \frac{\partial A_S}{\partial z} + \frac{\mathrm{i}}{2k_S}\nabla_\perp^2 A_S + \frac{\mathrm{i}k}{2}\left(\frac{n^2}{n_0^2} - 1\right)A_S = -\frac{\mathrm{i}}{2}\,p^* A_L, \tag{23}$$

$$\frac{1}{2\mathrm{i}\Omega}\,\frac{\partial^2 p}{\partial t^2} + \left(1 + \frac{1}{\mathrm{i}\Omega\tau}\right)\frac{\partial p}{\partial t} + \frac{p}{\tau} = -\frac{\mathrm{i}g}{\tau}\,A_L A_S^* + S\,, \tag{24}$$

where $k = k_L \cong k_S$, $\tau = 2/(\Gamma q^2)$ is the hyper-sound relaxation time (or the phonon lifetime),

$$g = \left(\frac{Y}{n_0 c}\right)^2 \frac{\omega\tau\Omega}{4\rho_0 v_s^2} = \left(\frac{Y}{n_0 c}\right)^2 \frac{n_0\omega^2\tau}{2\rho_0 c v_s} \tag{25}$$

is the SBS gain coefficient. In practice, the experimentally determined hyper-sonic decay time is often used, as it proves to be more accurate than estimates based on gas-dynamic constants.

In (22)–(24), the slowly varying refractive index is denoted by n, and the constant average value of the refractive index is distinguished within it, denoted by n_0 and determined from the relation $k_L = n_0\omega_L/c$. The field amplitudes in (22)–(24) are multiplied by $\sqrt{n_0 c/8\pi}$, i.e., normalized such that the radiation flux densities (in W cm^{-2}) are equal to $J_L = |A_L|^2$, $J_S = |A_S|^2$. The amplitude of the pressure change p in the hypersonic wave is multiplied by the quantity $Y\beta_s\omega_L/(2n_0 c)$; hereinafter, we will refer to it as the hypersonic amplitude.

Furthermore, the system of equations (22)–(24) describes the amplification of Stokes radiation, which arises in the medium as a result of the scattering of the laser field on chaotic thermal pressure fluctuations. In this regard, by analogy with (10), the delta-correlated Langevin force S [36, 37] is phenomenologically introduced into the equation for the hypersound amplitude (24).

In the field equations (22) and (23), in addition to the amplification due to the parametric oscillation of hypersonic waves, refraction is taken into account due to inhomogeneities in the refractive index n that are not related to density variations in the hypersonic wave. Refraction can be either linear or nonlinear, where n depends on the intensity of the laser and Stokes radiation.

The nature of the interaction between the laser wave and the SBS medium depends significantly on the ratio of the characteristic times of the problem. Let τ_c be the characteristic time of the change in the amplitude of the laser wave. Two characteristic times are associated with the medium: the period of hypersonic oscillations $T = 2\pi/\Omega$ and the hypersonic relaxation time τ. As follows from the above, the characteristic values of T lie in the range from tens of picoseconds to a few nanoseconds. In typical situations, T is much smaller than τ, since otherwise the hypersonic wave would decay before it has time to form. Therefore, equation (24) describes the SBS of relatively short or broadband laser pulses, where τ_c is comparable to or does not significantly exceed τ. For longer or narrow-band laser pulses with durations exceeding ten nanoseconds, the time τ_c may significantly exceed τ. In that case, the values of A_L, A_S and p will vary slowly against the background of oscillations not only of light fields but also of hypersonic wave, and equation (24) can be simplified by neglecting the term with the second derivative and using the condition $(\Omega\tau)^2 \gg 1$:

$$\frac{\partial p}{\partial t} + \frac{p}{\tau} = -\mathrm{i}\,\frac{g}{\tau}\,A_L\,A_S^* + S\,. \tag{26}$$

The correlation characteristics of the Langevin force and the random initial conditions p_0 and $\dot{p}_0$ must be such that, in the absence of radiation in the medium, the average level of hyper-sound amplitude fluctuations and their correlation time at every point in space remain constant over time. This is determined by the relations [32–35]:

$$\left\langle p_0(\mathbf{r}_1, z_1) p_0(\mathbf{r}_2, z_2)\right\rangle = 4\kappa F_s(\mathbf{r}_1 - \mathbf{r}_2)\delta(z_1 - z_2)\,,$$

$$\left\langle \dot{p}_0(\mathbf{r}_1, z_1) \dot{p}_0(\mathbf{r}_2, z_2)\right\rangle = \Omega^2 \left\langle p_0(\mathbf{r}_1, z_1) p_0(\mathbf{r}_2, z_2)\right\rangle,$$

$$\left\langle p_0(\mathbf{r}_1, z_1) \dot{p}_0(\mathbf{r}_2, z_2)\right\rangle = 0\,,$$

$$\left\langle S(\mathbf{r}_1, z_1, t_1) S^*(\mathbf{r}_2, z_2, t_2)\right\rangle = \left(\frac{2}{\tau}\right)\left\langle p_0(\mathbf{r}_1, z_1) p_0(\mathbf{r}_2, z_2)\right\rangle \times \delta(t_1 - t_2)\,,$$

where κ is the spontaneous scattering coefficient of laser radiation, measured in $\mathrm{cm}^{-1}\ \mathrm{sr}^{-1}$, and $F_p(r_1 - r_2)$ is the dimensionless correlation function that yields the unit brightness for Stokes radiation resulting from spontaneous scattering. The coefficient κ is taken from experimental data or estimated from the expression for the gaseous medium as $\kappa = 4\pi^2(n_0 - 1)^2/(\lambda^4 N_0)$, where N_0 is the concentration of gas molecules [38].

A model with similar capabilities, but based on the mode expansion of light fields, is described in [39]. In [39], the case of long laser pulses (equation (26)) is considered, and studies of the SBS are conducted, similar to those in [32]. Their results are consistent with the data in [32].

Equations (22)–(24) or (22), (23), (26) describe SBS in isotropic media with different refractive indices; however, the following discussion focuses on gaseous media for which the condition $n \cong n_0 \approx 1$ holds. In this case, the system of equations for SBS of the long narrowband pulses (22), (23), (26) has much in common with the system of equations for laser amplification (9), (10). The similarity of the equations for polarization (10) and hypersonic amplitude (26) is due to the fact that the speed of light is significantly higher than the speed of sound, and the motion of the hypersonic wave can be neglected during the interaction times of interest to us.

3. Nonlinear adaptive optics

The PC schemes in double-pass pulsed lasers of any type share many similarities; the review of research on laser systems with PC at SBS can be found in [40]. As an example of a high-power laser, we will consider the explosive photodissociation iodine laser (EPDL). It was developed at the dawn of quantum electronics and, in many ways, defined the horizons of its development in terms of achieving the ultimate pulse energy of laser devices.

3.1 Explosive photodissociation iodine laser

Research on EPDL pumped by the light from the front of shock wave (SW) began in the mid-1960s at the initiative of N.G. Basov, Y.B. Khariton, Y.B. Zeldovich, and S.B. Kormer. The EPDL has unique characteristics in terms of energy and, consequently, potential radiant intensity.

The EPDL is an atomic iodine gas laser whose initial active medium consists of perfluoroalkyl iodides C_3F_7I, C_2F_5I, CF_3I. The idea of exciting atoms through the photodissociation of more complex molecules when irradiated with the light beam belongs to S.G. Rautian and I.I. Sobelman (1961); the detailed description of the kinetics of the iodine laser is contained in the monograph [41]. The ground configuration of the iodine atom, $5s^2 5p^5$, is partially filled and yields two fine-structure states, $^2P_{1/2}$ and $^2P_{3/2}$, in *LS*-coupling terminology. The mechanism of active medium pumping is based on the photodissociation of the perfluoroalkyl iodide molecule upon absorption of light radiation in the spectral region with the central frequency of about 270 nm and the width of about 40 nm. As a result of photodissociation, an iodine atom is cleaved off, ending up in the $^2P_{1/2}$ excited state, with the quantum yield close to unity for the entire absorption band, especially for C_3F_7I. Laser radiation is generated in the $^2P_{1/2} - {}^2P_{3/2}$ transition of the ground electronic configuration. The transition is the magnetic dipole one, since the electric dipole transition is forbidden by parity, so the upper laser level is quite stable. This allows excited atoms to be accumulated in the $^2P_{1/2}$ state and then to generate the short pulse of stimulated emission. The upper laser level is split into two sublevels of the hyperfine structure with the quantum numbers of total angular momentum $F = 3$ and 2 (the spin of the iodine atom's nucleus is 5/2). The lower laser level, accordingly, is split into four sublevels with $F = 4$, 3, 2, and 1. The selection rule $\Delta F = 0, \pm 1$ results in the spectrum of six lines. The strongest line in the spectrum lies between the upper $F = 3$ and lower $F = 4$ sublevels ($\lambda = 1.315$ μm).

The pumping radiation source for EPDL is the front of SW propagating through the gas at high luminous temperature following the detonation of a specially configured explosive. The high energy density of the explosive and the source temperature make the SW front a more effective mechanism for creating population inversion compared to lamp sources [42] and allow for the pumping of large volumes of medium. SWs in noble gases are characterized by maximum brightness. The active medium can be added directly to the noble gas. Variants of EPDL on the C_3F_7I with pumping by the light of the front of SW with active region diameters of 150 mm, 500 mm, and 1200 mm are shown in Fig. 1. The first two variants, 'converging' and 'diverging' (based on the SW type), allow for output energies of 1 kJ and 50 kJ, respectively. The cross-section of the 'converging' type of EPDL is shown in Fig. 2. In the third

Figure 1. Modifications of EPDL with the diameter of active region of 150 mm (a), 500 mm (b) and 1200 mm (c).

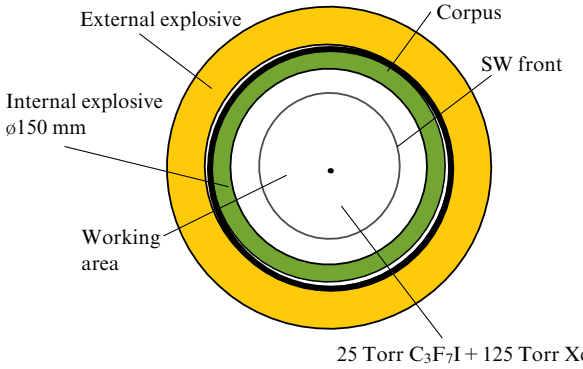

Figure 2. Cross-section of the 'converging' EPDL modification with the diameter of active region of 150 mm.

variant, the record-high radiation energy of up to 1 MJ was achieved [43]. By ensuring the diffractive divergence of the EPDL, the radiation flux of $\sim 10^{18}$ J sr^{-1} can be achieved.

To date, the EPDL remains the world's highest-energy single-channel laser. However, the challenge lies in realizing its enormous potential, as the divergence of the radiation from the powerful EPDL-generator significantly exceeded the diffraction limit. In the case of the EPDL with an energy of ~ 1 MJ and the active medium length of 30 m, the beam quality was pure, with half of the energy contained within an angle of $\sim 10^{-2}$ rad. The beam divergence was thus $\sim 10^4$ times greater than the diffraction limit.

The radiation pattern of optical lasers and methods for reducing it depend on the nature of optical inhomogeneities [44, 45]. A large number of studies have been devoted to optical inhomogeneities in iodine lasers [46–58]. Analysis has shown that the main cause of the large divergence of the EPDL-generator is the presence of the refractive index gradient in the SW front. In the case of EPDL with an energy of ~ 1 MJ, the refractive index gradient in the photodissociation layer in the front of SW reaches $\Delta n \approx 2 \times 10^{-6}$. The experimental divergence of $\sim 10^{-2}$ rad is explained by significant 3D effects of ray deflection in the active medium with the nonuniform gain zone and the focusing refractive index profile (G.G. Kochemasov).

It is clear that multiple passes of radiation through optically inhomogeneous active medium in the resonator contribute to an increase in divergence. Therefore, energy extraction per single pass or the use of nonresonant feedback in the resonator, where phase shift accumulation occurs chaotically and more slowly, appears to be more preferable for EPDL with large volumes of active medium. As a result, in the 'master oscillator (MO) + amplifier' and 'laser with an angular selector and nonresonant feedback' EPDL schemes with an output radiation energy of 0.1 MJ, it is in principle possible to reduce the divergence to $\sim 10^{-4}$ rad, i.e., by two orders of magnitude. This divergence is mainly determined by the angular deviation of the beam $L\nabla n$ after single pass through the medium of length L and is the limit for the laser without wavefront correction.

It is clear that simply increasing the length of the active medium L is ineffective, since with the linear increase in output energy as L increases, the radiation strength will decrease inversely proportional to L due to the linear increase in divergence $L\nabla n$. Increasing the amplifier aperture is also ineffective due to the challenges of manufacturing large-scale, aberration-free optical elements.

3.2 Phase conjugation at stimulated Brillouin scattering

The reduction in the divergence of the beam of EPDL can only be achieved through the use of adaptive wavefront correction. Linear adaptive optics are not applicable, since the temporal scale for changes in the refractive index of the medium is ~ 0.1–1 μs. Therefore, for wavefront correction, it is advisable to use methods based on nonlinear processes, such as stimulated scattering, three-wave, and four-wave interactions with relaxation times of 1–10 ns (see [1] and the references cited therein).

The most attractive approach is the compensation for optical inhomogeneities in two-pass laser amplifiers. For high-power lasers, the phenomenon of phase conjugation (more precisely, self-reversal) at SBS of laser radiation, discovered in the early 1970s by V.V. Ragulsky and colleagues and interpreted by B.Ya. Zeldovich, is of particular interest [6]. In the case of PC at SBS, the maximum reflection of the Stokes wave is observed in the opposite direction. Importantly, among all noise Stokes waves, the wave with the maximum amplification is the one that is complex-conjugate to the laser pump wave. This constitutes the essence of PC.

Thus, in a two-pass 'MO + amplifier' system, the MO laser emission with the flat wavefront passes through the amplifier and the optical path of the laser system, where it is amplified and distorted, then enters the SBS mirror, where it excites the reflected Stokes wave with the wavefront that is, ideally, complexly conjugate to the incident wave. The inhomogeneities of the reflected wave are thus automatically compensated during the return pass through the amplifier and optical path, eliminating the need for complicated system alignment. Due to the small frequency shift of the Stokes radiation, it does not exit the amplification spectral line. The possibility of achieving diffractive divergence of the laser with an optically inhomogeneous medium via the PC at SBS was proposed in 1971 (but published much later [59]) and demonstrated in the case of the ruby laser [60]. Furthermore, the PC phenomenon can encompass not only the laser

system but also the entire path from the laser to the distant target [61]. The fundamental feasibility of this approach was demonstrated by experiments [62, 63].

3.2.1 SBS-mirror with the random phase plate. The theoretical justification of the PC at SBS in [6] was of the qualitative nature. In reality, the radiation reflected from the SBS mirror is a combination of the conjugated wave and noise modes, whose contributions can vary significantly in different situations. The SBS-mirror consists of a SBS-active medium and a system for focusing laser radiation into this medium. It was standard practice to use a random phase plate in the PC mirror, located in front of the focusing lens [6–9, 64–66], with the help of which the PC phenomenon was discovered (see Fig. 3a).

After passing through such a plate, the laser beam, which originally had aberrations, acquires the small-scale speckled structure. The use of the SBS medium in the form of a long optical fiber to ensure multiple pump reflections from its walls allows for minimal noise and near-to-ideal PC quality (the gain coefficient of the conjugated wave is twice that one of the nearest nonconjugated modes), as demonstrated by experiments and calculations in the approximation of the steady-state linear SBS [67–71] and the saturated SBS [72, 73]. However, with significant radiation fluxes of the high-power laser, the problem of the optical fiber's radiation strength arises. To overcome this, it has been proposed to focus the laser speckled beam into a cell containing the liquid or gaseous SBS medium, i.e., to implement PC in focused beams [74, 75] (see Fig. 3b). However, the bell-shaped envelope of the laser beam is more pronounced in the Stokes beam. As the initial analysis showed, this leads to the increase in the role of noisy Stokes modes and the decrease in the PC quality, especially in near-threshold conditions of SBS, when the gain is linear [76–78] (the excess in the gain coefficient of the conjugated wave over the nearest nonconjugated modes is no longer twofold, but one and a half times). Although the nonconjugated modes experience less amplification, their large quantity significantly reduces the PC quality, characterized by PC coefficient in the form of the normalized overlapping integral:

$$h(z,t)=\frac{\left|\iint A_L(\mathbf{r},z,t)A_S(\mathbf{r},z,t)\,\mathrm{d}\mathbf{r}\right|^2}{\iint\left|A_L(\mathbf{r},z,t)\right|^2\mathrm{d}\mathbf{r}\iint\left|A_S(\mathbf{r},z,t)\right|^2\mathrm{d}\mathbf{r}}\,. \qquad (27)$$

In experiments conducted in the 1980s to compensate for diffraction divergence in high-power double-pass EPDL systems [79], this goal was not achieved. The reason was mainly that, using the classical approach to the focusing system, it was impossible to create the laser field structure in the SBS medium that was optimal for the selection of the conjugated Stokes component.

The clear dependence of the performance of the double-pass laser with PC on laser parameters and focusing characteristics necessitated more detailed studies of the behavior of SBS mirror itself, which began to be widely conducted using pulsed laser pumping in the nanosecond and microsecond ranges under laboratory conditions [80]. Experimental testing of the SBS mirror, especially in the case of powerful and specific systems such as the EPDL laser, is difficult without the development of the computational and theoretical framework. All of this initiated the transition to an in-depth computational and theoretical study of SBS in focused beams. Such an analysis must include aspects such as multidimensionality, SBS saturation, and nonstationary transient processes associated with the finite hyper-sound relaxation time. At the outset, simplified systems of SBS equations were solved, allowing for the consideration of two main classes of problems.

In the first class of problems, the emphasis was on accounting for the multidimensionality (initially 2D, and later 3D) of the medium, but under conditions of linear (unsaturated) SBS [81–85] and in the steady-state approximation. Ignoring saturation is an idealization, since in experiments it manifests itself to some extent almost always; moreover, operation in the saturated regime is one of the goals of the experiment, as this increases the reflection coefficient of the SBS mirror. The limitations of this approach were overcome in models that account for SBS saturation [86–94], but in steady-state conditions and most often for the 2D case.

In the second class of problems, the emphasis was placed on accounting for nonstationarity, but this came at the expense of multidimensionality. Nonstationarity begins to have an effect if the duration of the laser pulse or its rise time does not significantly exceed the relaxation time of the hypersonic wave. Since the latter lies in the range of a few to tens of nanoseconds for most liquids and gases of interest (see, e.g., [95]), the inclusion of nonstationarity in the model in most cases automatically implies the consideration of transient processes associated with the finite relaxation time of hypersound. The consideration of nonstationarity, which is also necessary for better understanding of the SBS process, was implemented in 1D transient models of both linear SBS [96, 97] and saturated SBS [98–102]. In 1D problems, it is possible to estimate the energy characteristics and temporal structure of the Stokes radiation as a function of the parameters of the active medium, but it is impossible to investigate the transverse structure of the light beams, which constitutes the essence of the PC.

In the numerical and theoretical model and computer code for the nonsteady-state SBS [32–35], which takes into account the main physical effects, it became possible to get closer to experimental situations. The model is based on the solution of nonsteady-state parabolic equations for the laser and Stokes fields (22), (23) and the nonsteady-state equation for the hypersonic amplitude of both the first (26) and second (24) orders. In the latter case, it is possible to study the SBS of short pulses or broadband radiation. The model accounts for transient processes, the 3D nature of the medium, the random source of hypersonic noise in the volume, diffraction, refraction, parasitic absorption, and self-action of radiation

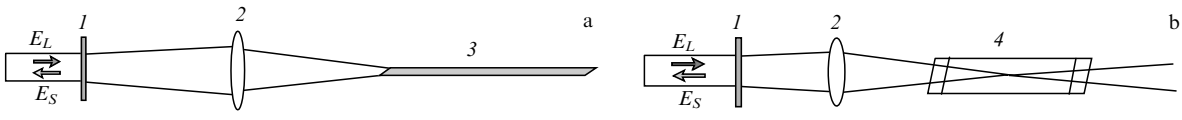

Figure 3. PC scheme with SBS-medium in the lightguide (a) and bulk cell (b): *1* — random phase plate, *2* — focusing lens, *3* — lightguide, *4* — bulk cell.

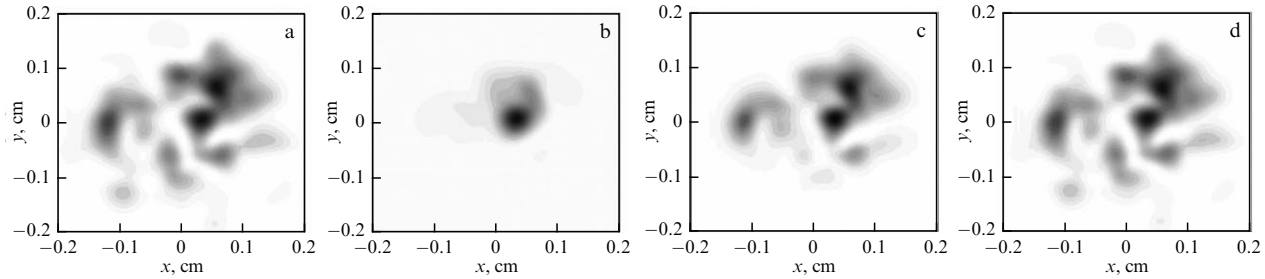

Figure 4. Transversal distribution of laser J_l at $\xi = 5$ (a) and Stokes intensity J_S for $R = 3\%$, $h = 45\%$ (b); $R = 63\%$, $h = 68\%$ (c); $R = 94\%$, $h = 88\%$ (d) at the SBS cell input.

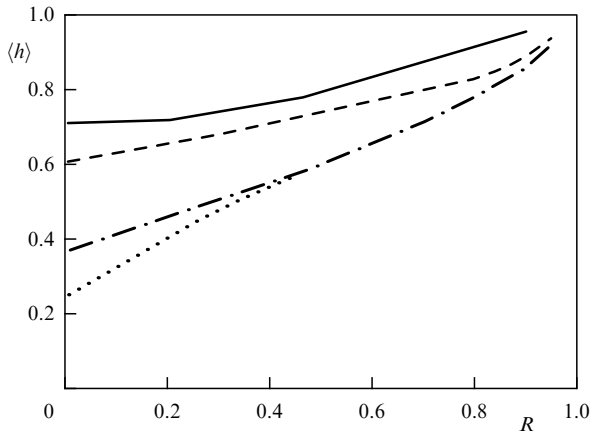

Figure 5. Dependence of average PC fidelity h against the reflection coefficient of laser radiation R at the excess of divergence over the diffraction limit $\xi = 1$ (solid line), $\xi = 2$ (dash line), $\xi = 5$ (dash-dot line) and $\xi = 10$ (dotted line).

(thermal self-focusing and strictive self-focusing), as well as the influence of Stokes radiation on laser radiation (SBS saturation).

Nonsteady-state 3D calculations of the SBS in focused beams [32–35] made it possible to investigate the process of Stokes radiation formation from the noise stage to deep saturation of the SBS and yielded results concerning both fundamental and practical aspects of PC. Figure 4 shows the transverse flux density distributions of the laser and Stokes radiation at the SBS cell input at various points in time, at which the corresponding PC coefficient h and reflection coefficient R are observed. The divergence of the laser radiation in $\xi = 5$ times greater than the diffraction limit. At the near-threshold stage of linear SBS, the Stokes beam is 'drawn' into the bright pump speckle due to exponential amplification, and only at deep SBS saturation does it approach the laser beam. The calculations confirmed the special role of SBS saturation in obtaining high-quality of PC, which are formed near the cell's input window, where the most active transfer of laser energy into the Stokes wave occurs. It was shown that physical processes that reduce the reflection coefficient R (defocusing aberrations, thermal self-defocusing, the influence of transient processes during the short pulse) decrease the PC coefficient h. Conversely, processes that increase R (focusing aberrations, striction self-focusing) also increase h.

It has also been shown that the presence of the hypersonic noise source in the SBS medium prevents the realization of the strictly stationary reflection regime under constant pumping — the Stokes radiation parameters exhibit rare and deep fluctuations over time. The cause of these perturbations is in the instability of the hypersonic lattice born in the laser beam waist. The phase of the hypersonic lattice is disrupted due to rare large fluctuations of hypersonic noise near the waist; subsequently, the phase disturbance shifts toward the input window, resulting in the formation of new hypersonic lattice.

Calculations have shown that, for a given laser radiation reflection coefficient, the PC quality monotonically (contrary to earlier assumptions [6]) decreases with increasing laser pump divergence, and at the fixed laser divergence, it monotonically increases with increasing reflection coefficient (Fig. 5). The main conclusion of the calculations is that in the near-threshold regime of linear SBS, the PC efficiency of focused laser beam does not exceed 60–70% for an ideal Gaussian beam and decreases significantly in the case of distorted beams (it is precisely for their correction PC is intended). The PC quality close to the ideal ($h > 90\%$) is achieved only at high SB saturation ($R > 90-95\%$), when there is the risk of competing parasitic nonlinear processes developing in the SBS medium (Stimulated Raman scattering, self-interaction, optical breakdown) [64–66]. It is therefore clear that achieving the high-quality of PC in SBS mirror with the random phase plate for the wide range of laser powers is problematic.

3.2.2 SBS-mirror with the raster of microlenses. The basis for improving the SBS mirror was provided by experimental studies of the configuration [103, 104], in which an ordered phase plate (a microlens array) was used instead of a random phase plate [6]. Each microlens was made in the form a Fresnel two-level zone plate [105]. In the case of the regular array, it is possible to controllably vary its characteristics, which broadens the range of conditions for focusing the laser pumping into the SBS cell.

In the SBS mirror scheme shown in Fig. 6a, laser radiation with divergence θ_L is introduced into the spatial filter (confocal angular selector), in the pinhole plane of which angular selection of the radiation takes place. The selector's transmission angle ($\theta_{\text{sel}} > \theta_L$, so the laser radiation passes through the selector without being cut off. The laser beam then passes through the ordered array of microlenses with the square packing and microlens diameter d. Next, a main lens with focal length F focuses the laser beam into the SBS cell. After passing through the array, the laser intensity exhibits characteristic distribution features in two spatial regions: the focal regions of the focusing lens (zone I) and the small lenses of the array (zone II) (see Figs 6a and 6b).

While with the random-phase plate the Stokes beam in the far zone consists of a narrow peak with the conjugated component and the wide-angle nonconjugated wing, in the

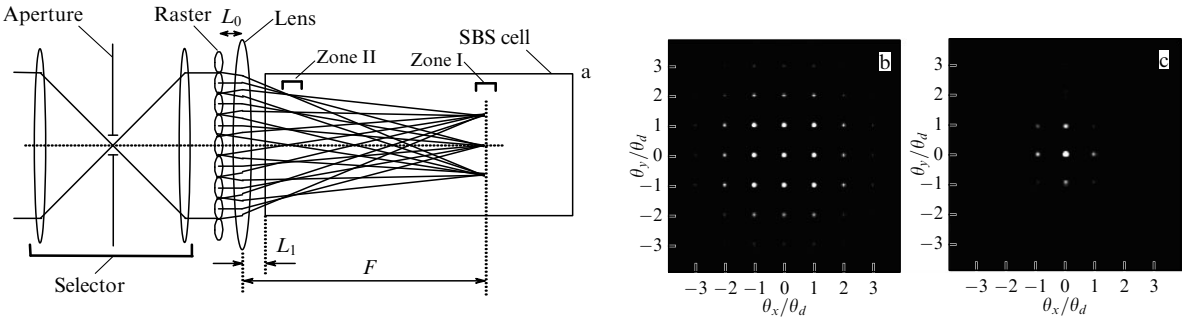

Figure 6. SBS-mirror scheme with the microlens raster (a) and typical picture of laser intensity in I zone (b) and Stokes intensity in the plane of selector pinhole (c).

case of the microlenses' raster the Stokes the radiation forms the pattern of equidistant narrow peaks (see Fig. 6c). The central peak contains the conjugated component, while the side radiation peaks are cut off by the angular selector.

A series of experiments on the EPDL with SBS mirror involving the microlens raster demonstrated the possibility of improving the beam directionality in the 'converging' EPDL configuration with the amplifier working aperture of 150 mm in diameter [106–108]. However, the system operated instably, and the radiation Strehl ratio was low.

Calculations have shown that the PC quality is highly sensitive to the position of the SBS cell relative to the focusing lens [109] (see Fig. 7). Analysis of the calculated data revealed the effect of record-low noise in the Stokes beam. The essence of this effect is that angular selection of the Stokes radiation allows for achieving nearly ideal PC quality if the input window of the SBS cell is located in the specific intermediate region between zones I and II. There, the periodic distribution of laser intensity is formed, which is practically independent of the nature of large-scale (compared to d) distortions of the laser beam [109] (see Fig. 7). The PC fidelity of the selected Stokes radiation in this case exceeds 90–95% at any laser intensity, starting from the threshold one. Displacement of the SBS cell from its optimal position leads to the noticeable decrease in the PC coefficient (7). Thus, in the optimal configuration of the SBS mirror, the central Stokes peak in the far field in Fig. 6 is as close as possible to the reflected component.

The experimental data were in full agreement with the results of SBS calculations of the selector's transmission and reflection coefficients [110, 32, 33] and of the PC quality [111, 112]. The experiments used ultra-clean SMBS cells (fabricated with using electron-beam welding, indium spacers) with the high-pressure gas mixture (tens of atm Xe + 1.5 atm SF_6). The 8- and 16-level kinoform microlens arrays had the working aperture of 100 mm with minimal microlens size of 120 μm.

To increase the selection coefficient, the configuration of the SBS mirror was optimized such that the focal regions of the small array lenses and the main lens are arranged in the SBS cell in reverse order [111]. This configuration allows for maintaining excellent image quality of PC and increasing and stabilizing the selector's transmission coefficient [113]. Quality of PC remains high regardless of nonstationary conditions [114] and the nature of distortions in the laser beam incident on the array.

Using the developed SBS mirror, diffractive divergence was demonstrated in a two-pass pulsed-periodic Nd:YAG laser under laboratory conditions without temporal degradation, thanks to the PC [114]. The PC of two- and four-channel pulsed laser beams was demonstrated under nonsteady-state SBS in the two-pass Nd:YAG laser amplification scheme under laboratory conditions [115].

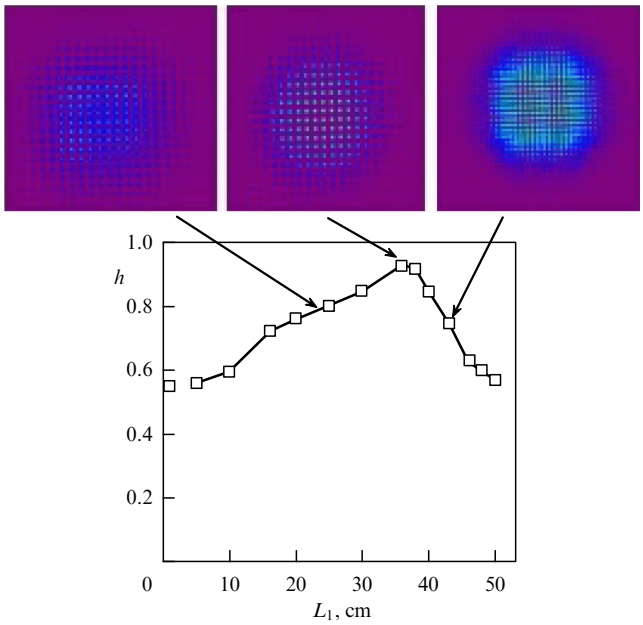

Figure 7. Calculational dependence of PC fidelity h after the selection (squares) against the distance between the focusing lens and SBS-cell L_1 under linear gain. Above the experimental laser pump distributions are shown in transverse planes indicated by arrows.

3.3 Explosive photodissociation iodine laser with phase conjugation

A schematic diagram of the EPDL laser with SBS mirror is shown in Fig. 8. The EPDL with the laser mixture of 25 Torr C_3F_7I and 125 Torr Xe is the two-pass laser system operating on the 'MO + power amplifier' principle. In experiments [106–108], the laser amplification cascade consisted of two amplifiers, A1 and A2. The length of the amplifiers and the distance between them, L_{12}, are subject to optimization. The SBS mirror is located at a distance L_{23} from the right end face of amplifier A2, which is closest to it. Due to the features of EPDL laser, the distance L_{23} is sufficiently large (several tens of meters) to reduce the probability of damage of the optical elements of the selector and diagnostic equipment by fragments during an explosive charge detonation.

During the first pass of the radiation through the path, its wavefront becomes distorted due to optical inhomogeneities in the active medium, aberrations of wide-aperture optical

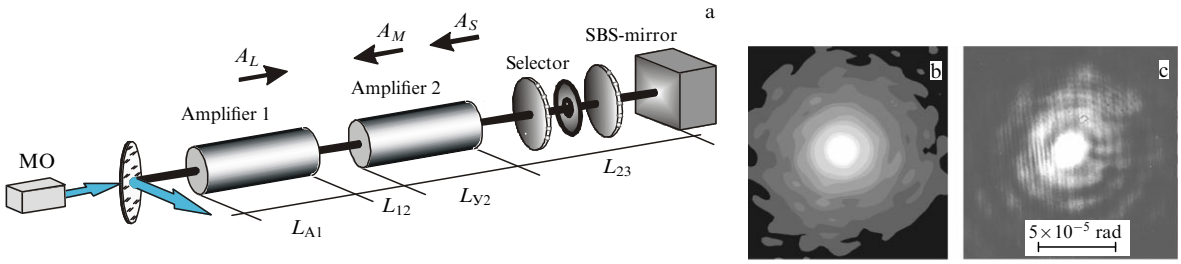

Figure 8. The scheme of two-pass EPDL with SBS-mirror (a) and EPDL energy distribution in the far field in calculation (b) and experiment (c).

elements, and atmospheric turbulence. The SBS mirror reflects the Stokes radiation field, which has the phase front that is complexly conjugate to the laser field at the input of the SBS mirror. The selector cuts off the high-angle unconjugated component of the Stokes radiation. Thus, while the Stokes wave is amplified in amplifiers A2 and A1, the effect of the amplifiers' optical inhomogeneities is simultaneously compensated. As a result, the output amplified Stokes radiation has the same beam quality as the MO radiation beam, i.e., close to diffractive quality. The radiation is extracted from the system using spatial decouplings. This is the ideal operating scheme of the EPDL, but under actual conditions a number of circumstances arise that degrade performance.

An analysis of the experimental setups for EPDL using the SBS mirror with microlens array [106–108], taking into account the newly discovered characteristics of PC [109–114], showed that the configuration of the SBS mirror in those experiments was not optimal. However, the instability of the intensity and Strehl ratio of the output radiation in the experiments [106–108] may stem not only from the nonideal operation of the SBS mirror, but also from other causes. Among these is the nonstationarity of optical inhomogeneities in the amplifiers, which leads to inaccuracies in their compensation even with ideal operation of the SBS mirror. Furthermore, there may be amplification of intrinsic spontaneous emission in the amplifiers, which can play a role under weak input signals. Finally, diffuse-mirror parasitic reflections of radiation on the windows of the amplifiers and other elements are possible, leading to self-excitation of the amplifiers under conditions of high EPDL gain. Consequently, an A_M wave with high divergence is formed in the laser system, which propagates in the direction opposite to the A_L field, i.e., in the direction of the A_S field (see Fig. 8a). As calculations have shown, the most dangerous in terms of parasitic reflections are the right window A2, the left window A1, the optical elements of the selector and SBS mirror. The high gain in the laser medium leads to the A_M parasitic wave being amplified quite significantly and depleting the population inversion while the useful signal propagates from the amplifiers to the SBS mirror and back. Moreover, the reflection of the parasitic A_M wave at the left window of amplifier A1 results in the significant parasitic component being added to the input laser signal.

All these aspects significantly complicate the understanding of how the EPDL operates, making reliable computational modeling of the entire EPDL system with the SBS mirror essential. In the case of the EPDL in the 'converging' configuration (Fig. 1a and Fig. 2), the relaxation time τ_2 is ~ 1 ns; therefore, for pulse durations in the microsecond range, the transient processes in (9) can be neglected. Additionally, an equation of type (9) must be added for the A_M parasitic wave.

The equations for field amplitudes must be supplemented by the system of equations for population states in the balance approximation, from which the gain coefficients α_L and α_S for equations (9) are determined. Detailed modeling of the population kinetics, together with the solution of the transport equation, was carried out in a one-dimensional EPDL model [116]. This is complicated by the fact that the accuracy of the process constants used for specific conditions is low, which in some cases leads to significant discrepancies between the calculated energy results and experimental data. To overcome this difficulty, the system of local kinetic equations can be reduced to an equation for the inversion of population states ΔN (compare with (14)):

$$\frac{\Delta N(r,t)}{\mathrm{d}t} = \frac{\Delta \tilde{N}_0(r,t)}{\mathrm{d}t} - \frac{\Delta N(r,t)}{\hbar\omega}\left[\sigma_L(J_L+J_M)+\sigma_S J_S\right], \quad (28)$$

where $r^2 = x^2 + y^2$, $\Delta\tilde{N}_0$, is population inversion in the absence of generation, associated with the weak-signal gain coefficient. This quantity was measured experimentally by probing the amplifier at various points across its cross-section with the low-power beam.

The calculations the refraction of the radiation, parasitic reflections of the laser radiation from the ends of the amplifiers and optical components, the amplifiers' own amplified spontaneous emission, radiation losses in the optical path, gain inhomogeneity, and the refraction of radiation on optical inhomogeneities in the active medium caused by the SW are taken into account. It was assumed that the SBS mirror with the microlens array is in an optimal configuration and that the quality of the optical beam is ideal, based on studies [109–114]. The dependence of the SBS mirror's reflection coefficient on the laser power incident on the SBS cell was taken as given in [116]. The influence of the EPDL parameters (optical scheme geometry, level of parasitic reflections, MO signal power, SBS threshold power) on its operational efficiency was investigated. It was shown that in a lamp-pumped MO, parasitic reflections of laser radiation from the ends of the amplifiers and optical circuit elements with the coefficient exceeding 10^{-7} significantly reduce the output radiation intensity. Special experiments have shown that it is difficult to achieve parasitic reflection coefficients less than 10^{-6} in the system. Calculations have shown that to suppress the effect of parasitic reflections, the intensity of the MO radiation at the input to amplifier A1 must exceed 10–20 W cm^{-2}. Since the intensity of the lamp-pumped MO radiation is at the level of 1 W cm^{-2}, an explosive MO was created to meet this requirement. As a result of optimizing the EPDL, an angular divergence close to the diffraction limit was achieved at $L_{A1} = L_{A2} = 1$ m, $L_{12} = 20$ m, $L_{23} = 65$ m (Fig. 8a), with the output radiation Strehl ratio reaching 0.7 [117, 118] (Fig. 8b, c). At the same time, good agreement was

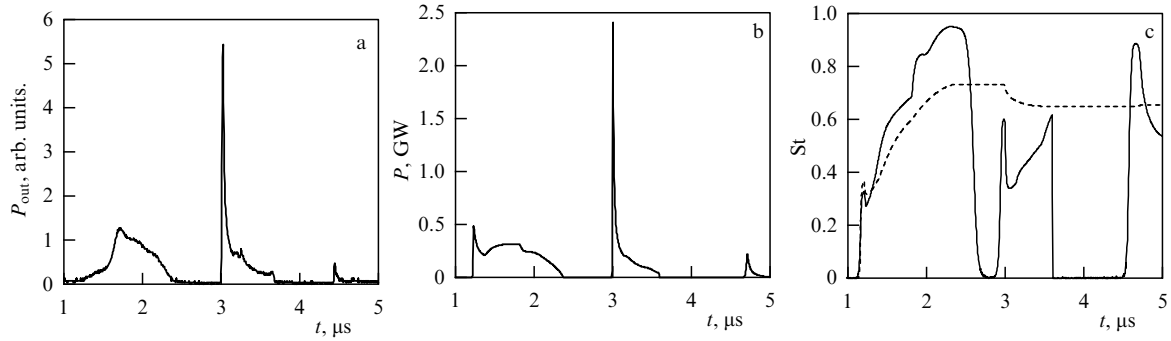

Figure 9. The dynamics of experimental (a) and calculational (b) power and calculational Stehl ratio (c) of EPDL radiation. Dynamics of averaged Stehl ratio is shown by dotted line.

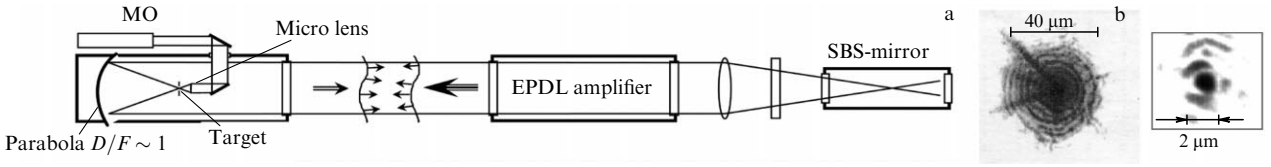

Figure 10. The experimental scheme of limiting focusing of EPDL radiation (a) and focused spot without (b) and with (c) PC.

obtained between the EPDL calculation results and the experimental data on energy, the time dependence of power, and the Strehl ratio (Fig. 9). Due to the threshold nature of the SBS, the pulsed-periodic mode is realized in the EPDL, where the pulse repetition period of the output radiation is equal to twice the time it takes for the radiation to travel from the amplifier to the SBS cell.

The application of PC in EPDL makes it possible to address the important issue of achieving ultra-strong electromagnetic fields of laser radiation. The standard approach is concerned with shortening the laser pulse, with femtosecond lasers. With an energy of 10 J, the pulse duration of tens of femtoseconds, and the focal spot size of 10 μm, an intensity of $10^{20}-10^{21}$ W cm^{-2} can be achieved. But there is another approach: to generate the relatively long pulse, but with large aperture and high energy, and to focus it into a spot of extremely small size (of the wavelength scale), using PC at SBS. The use of PC technology is key here. In this case, even with the fairly long pulse, the same intensity level can be achieved as with the standard approach. A number of attractive features emerge: the study of material behavior under quasi-stationary conditions (compared to characteristic atomic relaxation times), monochromatic irradiation, and the study of process dynamics.

Such an experiment was conducted using the EPDL with PC [119]. Its schematic diagram is shown in Fig. 10a. The reference weak beam from MO with the flat phase front entered a micro-objective (in fact, a microscope) from the back. The microlens formed the very small spot in its front focal plane. The radiation then passed to a parabolic mirror with a diameter-to-focal-length ratio of approximately 1. Next, the standard two-pass scheme with the PC was implemented. Images of the laser spots with and without the use of the PC at SBS are shown in Fig. 10b, c. The focal spot size with the PC is close to the wavelength. In the experiment, with the pulse duration of 1 ns and an energy of 100 J, the intensity on the target was 3×10^{18} W cm^{-2}, and the electric field strength was 5×10^{10} V cm^{-1}, which is significantly greater than the electric field strength in a hydrogen atom at the Bohr radius.

Advances in EPDL technology involve addressing key challenges, one of which concerns how to increase the energy and intensity of the radiation. As the potential of the active medium is exhausted, the main hope lies in the development of a multi-channel laser. If the radiation phase alignment (phasing) is ensured in N parallel channels, then in addition to an N-fold increase in power, the radiant intensity can be increased by a factor of N^2. And the PC is one of the mechanisms for combining lasers [115, 120, 121]. The second problem concerns the delivery of radiation to the receiver under conditions of an optically inhomogeneous propagation path.

When transitioning to the two-channel version of the EPDL, the SBS mirror allows for the natural implementation of coherent phase combining of the radiation: phasing is the special case of PC for a fragmented beam. The schematic diagram of the EPDL in the two-channel version is shown in Fig. 11 [122]. The MO was located in the turbulent atmosphere at 2.5 km from the input to the amplifier block; here, in the plane of the MO pinhole, the amplified Stokes radiation was detected.

The experimental setup was designed to ensure high-quality PC [109–114]. Two arrays of 8-level diffractive microlenses, each 1 mm in size and with the focal length of 9.5 cm, were used. Radiation intensity of approximately 4 W cm^{-2} was delivered at the input of amplification channels. The radiation propagation path was included in the EPDL calculation model. The model for calculating radiation propagation in the turbulent atmosphere is described in [123]. Calculations showed that, with the phase-matched input signal from the MO, the transition from one to two EPDL channels results in the 4.4-fold increase in radiant intensity in the absence of parasitic reflections from optical elements, and the 2.1-fold increase in output energy regardless of their influence. This is explained by the increased growth of the reflection coefficient of the SBS mirror with the twofold increase in the pump radiation power.

Figure 12a and b show the energy distribution in the near field of the radiation from MO, amplified after the first pass, and the Stokes radiation emerging from the SBS mirror

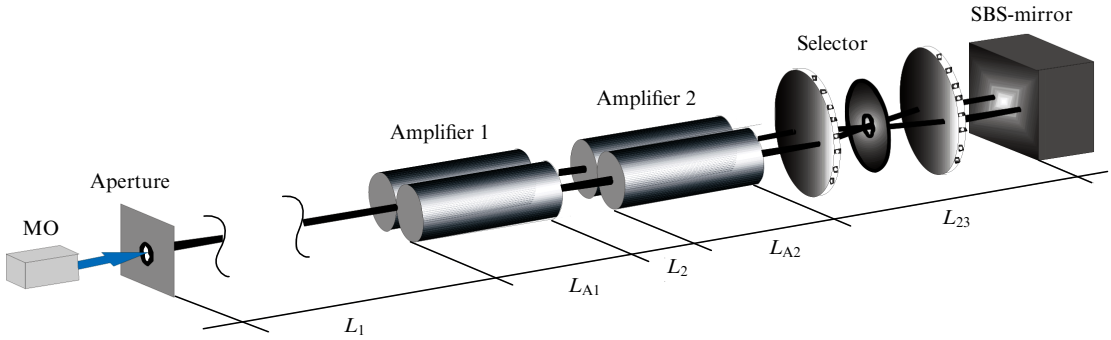

Figure 11. The scheme of the two-pass two-channel EPDL with SBS-mirror.

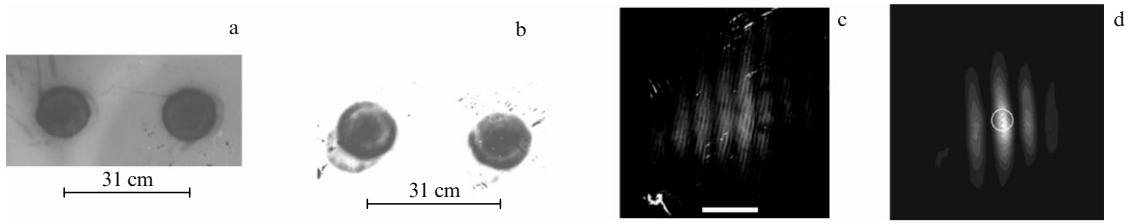

Figure 12. Experimental energy distribution of laser pump (a) and Stokes (b) radiation in near field and EPDL energy distribution in the MO pinhole plane in the experiment (c) and calculation at $C_n^2 = 10^{-15}$ cm$^{-2/3}$ (d).

before the second pass. The Stokes radiation reflected from the SBS mirror in the near field also consists of two circular spots separated by the same spatial interval that quite impressively symbolizes the essence of the PC.

The radiation from the two EPDL channels in the plane of the MO pinhole, at the distance of 2.5 km from the amplifier block, exhibits an interference pattern. The distance between the bands, $\Delta x = \lambda L_1/\delta$ where $L_1 = 2.5$ km and $\delta = 31$ cm equals about of $\Delta x \approx 1.0$ cm that is close to the experimental data. The total width of the distribution, which is determined by the radiation pattern from the single channel, and the period of the interference pattern in the experiment and calculation are in good agreement (Fig. 12c, d). The maximum brightness of the EPDL is observed on the optical axis regardless of the turbulence realization. The calculations show that replacing the SBS mirror by a conventional 100% reflective spherical mirror leads to significant beam blurring in the pinhole plane and its random shift.

3.4 Stimulated Brillouin scattering of vortex laser beams

In the study of the SBS process of focused laser beams with complex spatiotemporal structures, beams with screw dislocation of the wavefront (Laguerre–Gauss vortex modes) whose phase surface forms an Archimedean helix [124] are of particular interest.

$$A_L(r,\varphi,z) = A_0\,\frac{w_0}{w}\left(\frac{r}{w}\right)^m L_n^m\left(2\,\frac{r^2}{w^2}\right)\exp\left(\mathrm{i}m\varphi\right) \times \exp\left(-\frac{r^2}{w^2} + \frac{\mathrm{i}zr^2}{z_0 w^2} - \mathrm{i}\,(2n+m+1)\,\mathrm{arctg}\,\frac{z}{z_0}\right), \tag{29}$$

where $L_n^m(x)$ is the generalized Laguerre polynomial, and m is the topological charge of the optical vortex. The Laguerre–Gaussian mode LG_n^m (29) is the solution to equation (22) in the case of the homogeneous medium. Along the beam axis, the intensity is zero and the phase is undefined. When circling a singular point on the phase surface, it is impossible to return to the initial position. The presence of an optical vortex is determined by its interference pattern, for example, with an obliquely incident regular wave: a band emerges at the singularity point and a 'fork' is formed. Figure 13 shows laser beams LG_0^1 and LG_1^1 and their phase portraits with characteristic 'forks.' Vortex beams are of interest because chaotic vortices form during beam propagation in randomly inhomogeneous media [6]. Their correction is problematic using linear adaptive optics methods with the flexible adaptive mirror due to the discontinuous phase surface.

The theoretical analysis based on the perturbation theory and calculations for linear steady-state [125] and nonsteady-state [126] SBS of vortex laser beams directly focused into the SBS medium have shown that the PC of SBS in focused beams is not an universal phenomenon. The predicted phenomena observed at SBS of vortex beams were fully confirmed in experiments [127–129].

At first, it was shown that the PC of vortex beams is not observed due to the absence of selection of the conjugated Stokes mode, since the gain coefficients of this mode and a similar mode with reverse helicity are identical. For example, in the case of the simplest laser mode LG_0^1, the Stokes beam is essentially a random combination of the two modes LG_0^1 and LG_0^{-1}. The intensity distribution of the Stokes beam in the far field resembles the distorted $\sin^2(\varphi + \varphi_0)$, and the phase portrait indicates the presence of the wavefront edge dislocation (see Fig. 13a). To generate the LG_0^1 vortex beam [130], special kinoform spiral phase plates were developed [131].

Second, for the fairly broad class of vortex beams (for example, in the case of a laser mode LG_1^1 with two intensity rings), a phenomenon is observed that can be referred to as phase transformation at SBS. Its essence lies in the fact that a single mode is selected in the Stokes beam, but it is not the conjugate laser mode; moreover, it is orthogonal to it. In the SBS regime, which is close to linear one, the selected mode is the fundamental Gaussian mode LG_0^0; its regularity is preserved even at high SBS saturation. The regularity of the Stokes phase front in the experiment is evident from Fig. 13b.

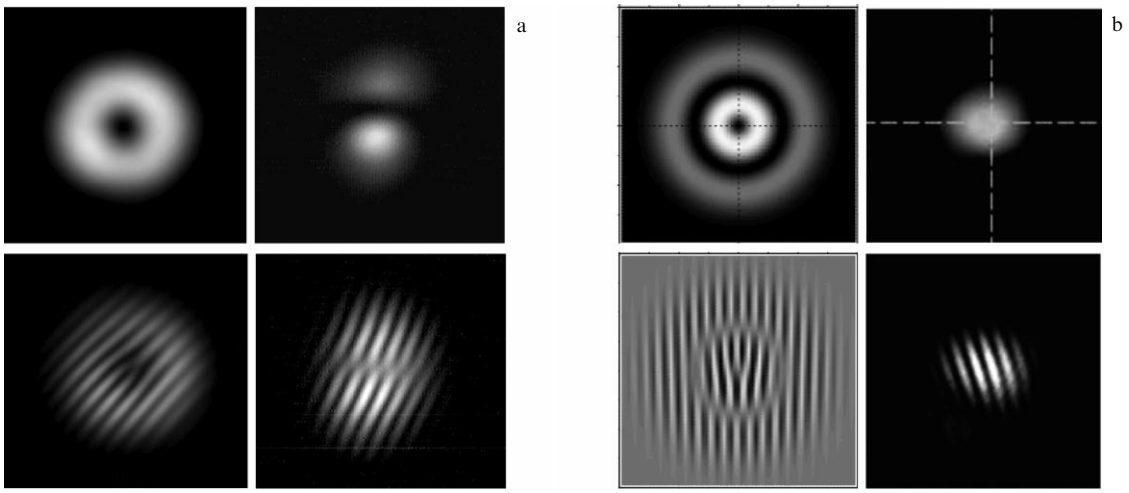

Figure 13. Laser LG_0^1 beam and Stokes beam (a) and laser LG_1^1 beam and Stokes beam (b) in the experiment. Intensity (top row) and phase portrait (bottom row).

The amplification coefficient of the LG_0^0 mode exceeds the amplification coefficient of the conjugated LG_1^1 mode and the LG_1^{-1} mode by 20% [125, 126], which ensures its selection. In the experiments the LG_1^1 vortex beam was formed at the output of the master oscillator using a tunable astigmatic $\pi/2$ converter based on an optical quadrupole [132].

As theory and calculations have shown, as n increases, the degree of selection of the fundamental Gaussian mode increases, and the ratio of the amplification coefficients of the fundamental mode LG_0^0 and the conjugated mode LG_n^m reaches 1.5. Moreover, the phase transformation effect can also be observed for nonvortex beams with $m = 0$ without an axial dip in the intensity distribution. Calculations have shown that during the SBS of vortex beams, vortex hypersonic waves are generated in the SBS medium, the structure of which is closest to that of the laser wave. Indeed, according to the $p \cong -igA_L A_S^*$ estimate based on (26), the phase structure of the hypersonic wave contains the central vortex with the same charge as the pump assuming that Stokes beam has the regular structure. The obtained result demonstrates the law of topological charge conservation: the total charge in the 'Stokes wave + hypersonic wave' system is equal to the charge of the input laser mode.

As for the PC, calculations and experiments [127, 129] have also shown that the high-quality PC of the vortex beams can be obtained in the SBS mirror with the microlens array (Fig. 7a) by disrupting the stable vertical beam structure.

4. Linear adaptive optics

As noted above, linear adaptive optics can be used for phase correction of continuous wave radiation and for pulses of approximately 1 ns or shorter. In continuous-wave lasers, real-time phase correction is possible only for relatively slow wavefront distortions. In the case of short pulses, adaptive phase correction is performed integrally over the pulse duration, i.e., in the static mode.

4.1 Coherent phase combining of multi-channel radiation

As noted above, when the active medium's potential is fully utilized, further increases in laser energy and power are possible only by combining multiple emission channels. However, the serial combination of channels has obvious drawbacks. Increasing the system's length leads to the accumulation of optical inhomogeneities, which degrade the quality of the output radiation. Moreover, heating and the occurrence of various nonlinear processes in the active medium can lead to its destruction. Therefore, it is clear that the creation of high-power laser systems is more effective when using parallel beam combining. Furthermore, it possesses the key advantage that is essential for applications: with N channels, the systems power and energy increase by the factor of N compared to the single-channel system, and the radiant intensity can be increased by the factor of N^2 due to the increase in the system's total aperture, provided that the radiation phases in the channels are strictly aligned (phased). Phase control in multichannel systems is achieved through phase shifting, assuming that the divergence of the radiation in each channel is close to the diffraction limit. For this type of phase control, electro-optical modulators [133], nonlinear optical elements [134, 135], piezo-optical devices, or other elements [136, 137] are used.

Recently, there has been rapid global progress in the development of continuous-wave solid-state lasers using active media in the form of doped slabs, discs, and fibers [138–140]. Fiber lasers are of particular interest due to their high efficiency and the ability to achieve relatively high power output despite the system's compact size [141, 142]. The power of a single-mode fiber laser of the order of 10 kW in the MO + amplifier configuration [143], appears to be approaching its limit due to increasing thermal loads and parasitic nonlinear effects [144–147]. To further increase the power, incoherent beam combining can be used [148–150], but to more radically increase the output radiant intensity, the beams from the channels must be combined in phase.

The feasibility of using the PC at SBS for the phasing of continuous-wave fiber lasers is being investigated [151, 152], with the high SBS threshold power posing the significant limitation. There are a number of linear approaches for the coherent summing of multi-channel continuous-wave radiation [153–155], including passive and active phasing. Passive methods (combining resonators, using Bragg gratings, etc.) are complex to align and construct and are designed for low laser power [156, 157]. Active coherent phasing includes methods with or without the determination of absolute or relative phase.

Coherent active phasing requires a single narrow-band, single-frequency laser MO source to ensure that phase fluctuations associated with the finite width of the laser spectral line are transmitted synchronously to all channels. The optical path length in the channels must be aligned with an accuracy that is significantly smaller than the coherence length of the MO radiation. The MO radiation is split, passes through phase modulators, and enters the amplifiers. After amplification, part of the radiation is directed via a splitter (light-splitting plate) to a device analyzing of output radiation in the channels. In phase-detection systems, the relative phases are analyzed, for example, using the heterodyne method with an additional channel. After the phases are determined, the required phase shifts are applied using phase modulators.

In the coherent combining scheme with active heterodyne phase control, the power of approximately 1 kW was achieved by summing the signals from five amplifiers [158]. The phase of each element was controlled by a lithium niobate phase modulator. An additional reference channel was frequency-shifted and interfered with the part of the signal from each channel. Detectors recorded the heterodyne modulation signal, and an electronic circuit measured the relative phase for each channel. In [159], the radiation of eight fiber amplifiers was combined, and the output power reached 4 kW. With coherent adding of five beams using a diffractive optical element (DOE) to combine the beams, an output power of 1.93 kW was obtained at $M^2 = 1.1$ [160]. In [161], the DOE was used to combine the two-dimensional array of 3×5 fiber amplifiers with an output power of 600 W at $M^2 = 1.1$. Using the DOE, an output power of 4.9 kW was achieved by coherent combining of the radiation from five fiber amplifiers with the power of 1.2 kW each [162]. The maximum number of channels (48) were also successfully summed using coherent active phasing [163, 164]. The limitation on the channel output power under coherent combining stems from the fact that the sufficiently narrow spectral line of the MO is required to ensure the desired coherence length; the narrower the line, the more effectively parasitic SBS is excited in the fiber.

It is worth noting that the principles of active coherent phasing are not limited to fiber lasers; they can also be applied to other continuous-wave laser systems [165]. The laser system [166] consisted of 7 amplification channels, each containing 4 amplifiers with thin Nd:YAG composite slabs end-pumped by diode arrays. Phase alignment was performed in each channel, followed by phase summation.

The conceptual simplicity of the heterodyne approach to coherent active phasing comes at the cost of the complex device architecture, largely due to the need to measure the phases at the system's output. Furthermore, such a system is highly sensitive to noise. It is also important to note that solving a number of practical problems requires focusing the radiation in an optically inhomogeneous medium through which the laser radiation propagates, such as the atmosphere. The turbulent atmosphere disrupts the phase structure of the multi-channel beam as it propagates, even if it was phase-aligned at the system output. Therefore, it is necessary to set the phase distribution at the output of channels that compensates for the optical inhomogeneities of the atmosphere along the radiation propagation path. Since the goal is to achieve a spot of minimal size (i.e., maximal intensity) at the remote receiver (target) under the unknown optical properties of the medium, the approach must be iterative,

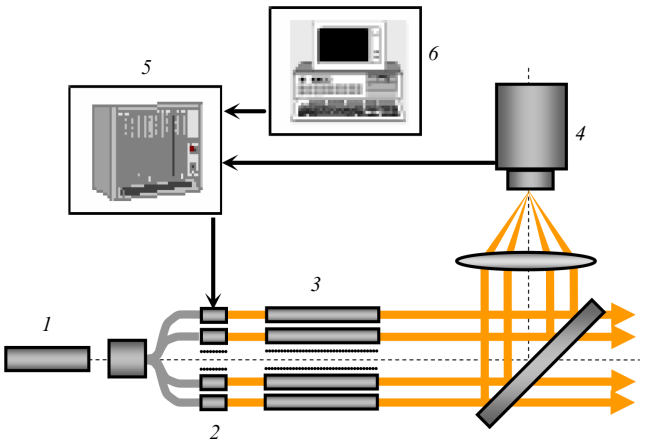

Figure 14. The scheme of coherent beam combining system: *1* — MO, *2* — phase modulators, *3* — amplifiers, *4* — single-element photodetector, *5* — control unit with microcontroller, *6* — computer.

involving the search for the extremum of the criterion functional (metric). Thus, the radiation receiver must be included in the feedback loop. If the target is located at relatively short distance and is cooperative, the feedback can be wired [134]. Otherwise, when irradiating the target in the feedback loop, the additional receiver is located near the emitting system and performs optical remote monitoring of the irradiation spot [167, 168].

Figure 14 shows the schematic diagram of the system for the iterative coherent combining of multi-channel laser radiation.

Since atmospheric distortions of the laser beam are dynamic in nature, there is the need for fast and reliable approaches to controlling phase shifts across the channels. This problem could be solved by active coherent methods without phase determination (gradient descent, hill climbing, genetic algorithms, etc.), but these methods have low operation speed. In this regard, the stochastic parallel gradient descent (SPGD) algorithm is of interest, whose concept was adapted from the theory of artificial neural networks [169, 170], where it is used in machine learning, to adaptive optics [171, 172] for controlling the flexible mirror, and only later applied to the phasing of multichannel radiation.

The paper [173] demonstrated coherent phase alignment over an atmospheric path approximately 400 m long using the cooperative target. In the work [174], coherent phase addition was performed for the first time in a 7-channel system of narrow-band, milliwatt-level fiber-optic ytterbium lasers in the feedback loop with the noncooperative target. The laser system was located at the height of 15 m, the radiation receiver (target) at the height of 40 m, with the distance between them of $L = 7$ km. With an individual output beam aperture size of $d = 3.3$ cm, the total aperture size was $D = 10.7$ cm. The operation of the SPGD-loop for controlling phase shifts at the frequency of 140 kHz was combined with relatively slow adjustment of wavefront tip-tilts in the channels at the frequency of 3 kHz. Naturally, at high operating frequencies, the phasing system employs a single-element photodetector of the metric, and the system is controlled not by the computer but by a microcontroller in which the algorithm program is 'hard-coded.'

The effectiveness of phasing is affected by both the spatial and temporal scales of radiation phase fluctuations in the

medium. In [175], using the model described in Section 2.2, it was demonstrated theoretically that the efficiency of phasing through the turbulent atmosphere is high when the atmospheric coherence radius (Fried parameter) [176]

$$r_0 = (0.423k^2C_n^2L)^{-3/5} \tag{30}$$

approximately equal to or greater than the transverse dimension of the laser channel, d. The structure constant of refractive index $C_n^2 = 6 \times 10^{-16}$ cm$^{-2/3}$ measured in [174] corresponds to the Fried parameter $r_0 = 8.4$ cm, i.e., significantly larger than d and close to D that indicates the weak influence of turbulence in the experiments [174].

In [177], the coherent combining formulated in [174] is demonstrated for a 21-channel system with the Fried parameter r_0 varying in the range from ~ 10 cm to ~ 1.5 cm, i.e., for $r_0/d \sim 3-0.5$. According to [175], the Strehl ratio St of the focused radiation is close to the ideal value at $r_0/d \geqslant 1$, and begins to decrease at $r_0/d < 1$, remaining at the sufficiently high level of St ~ 0.6 at $r_0/d \sim 0.5$. In [177], the conclusions [175] regarding the requirement for the spatial resolution of the coherent phase combining system were experimentally confirmed. At $r_0/d \sim 0.5$, the sufficiently high level of phase correction is achieved in the experiment. Interestingly, the Rytov dispersion, which characterizes the level of radiation intensity fluctuations in the statistically homogeneous atmosphere [178],

$$\sigma_R^2 = 1.23C_n^2k^{7/6}z^{11/6} = 2.91\left[\frac{z}{kr_0^2}\right]^{5/6} \tag{31}$$

lies in the range 0.17–4 for $r_0 = 10-1.5$ cm. When $\sigma_R^2 \geqslant 1$, as is known [178], the strong scintillation regime is realized, which allowed the conclusion to be drawn in [177] that phase correction of atmospheric turbulent distortions is achieved at coherent combining even under conditions of strong turbulence. In the strong scintillation regime, multiple optical vortices (see Section 3.4), speckles, and dark spots form in the laser beam. From the perspective of adaptive optics, the problem of strong scintillation lies in the difficulties of measuring the radiation wavefront. Thus, the 'blind' iterative SPGD approach, without wavefront measurement, allows for achieving a certain result even in the case of significant speckled structure of the beam.

In addition to the spatial resolution of the phasing system, its temporal resolution plays the significant role; the deficiency in this resolution leads to the decrease in the Strehl ratio. The SPGD correction in [177], as in [174], was performed at the frequency of 140 kHz, and the experimental values of the Strehl ratio obtained were lower than the calculated values. The phasing time, i.e., the convergence time of the SPGD algorithm, τ_{ph}, in [177] was 2–2.5 ms.

The SPGD algorithm, in its various forms, essentially consists of the combination of two stages of each iteration: the random stage and an 'intelligent' stage. In the first stage, small random phase shifts are applied to the channels, and in the second, 'intelligent' stage, corrective adjustments are made. The algorithm is based on the fact that the partial derivative of the metric with respect to each variable (i.e., phase in the channel) is, on average, directly proportional to the displacement of that variable and the change in the metric after the first stage. By optimizing the dynamic coupling between the parameters of the stochastic parallel gradient

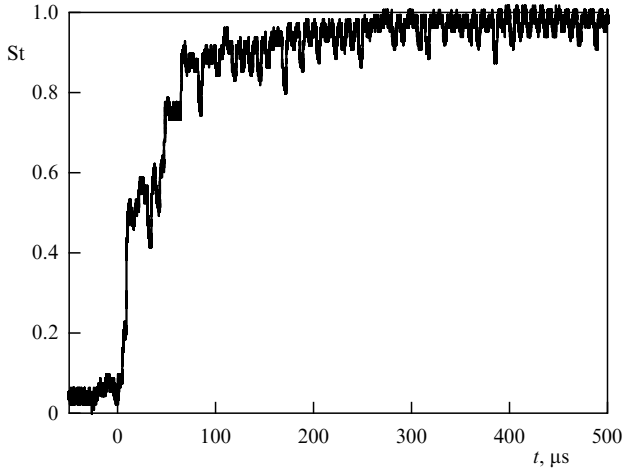

Figure 15. Experimental temporal dependence of Strehl ratio after the feedback activation.

(SPG) algorithm, conditions were found to increase the convergence rate of the metric to 2–3 iterations per laser channel [179]. In [180], SPG phasing of a 7-channel fiber laser system with compensation for its thermal distortions at the frequency of 14 kHz was experimentally demonstrated, and in [181], an operating frequency of 450 kHz was achieved. The phasing time τ_{ph} at the output needed for reaching the Strehl ratio of 0.8 is approximately 0.05 ms (see Fig. 15).

In [181], with the dramatic increase in the performance of the SPG phasing system, the influence of the time scale of phase fluctuations in the medium with dynamic optical inhomogeneities on the phasing of multichannel radiation was studied theoretically and experimentally. The criterion for phasing efficiency was established based on the ratio between the phasing time τ_{ph} and the characteristic time of change of turbulent phase fluctuations τ_{turb}. It is shown that the increase in the average Strehl ratio begins at $\tau_{turb}/\tau_{ph} \approx 2$, and the sharp increase in the efficiency of compensation for dynamic phase distortions along the propagation path occurs at $\tau_{turb}/\tau_{ph} \approx 20$. At $\tau_{turb}/\tau_{ph} > 20$, the average Strehl ratio remains at the constant level, the value of which is high if the coherence radius r_0 is of the order of or greater than the channel aperture size d.

4.2 Phase control with the help of flexible mirrors

Let us consider the configuration of the standard closed-loop adaptive optical system (Fig. 16a) with an adaptive mirror, which is its key optical element. The parameters of the adaptive system are largely determined by the capabilities and characteristics of the mirror used (see [182–185]). One of the main requirements for adaptive mirrors is the ability to compensate for the maximal number of aberrations using the minimal number of control actuators. Therefore, the main characteristic of any adaptive mirror is the response function of its actuators, i.e., the deformation of the corrector surface caused by the action of a single actuator while the control signals on the other actuators are zero. It is assumed that the total surface curvature is the superposition of deformations initiated by each actuator. Another characteristic of the adaptive mirror is the amplitude of the mirror surface's displacement. The Strehl ratio is commonly used as the criterion for correcting phase distortions. According to the Maréchal criterion [186], an optical system is considered well-

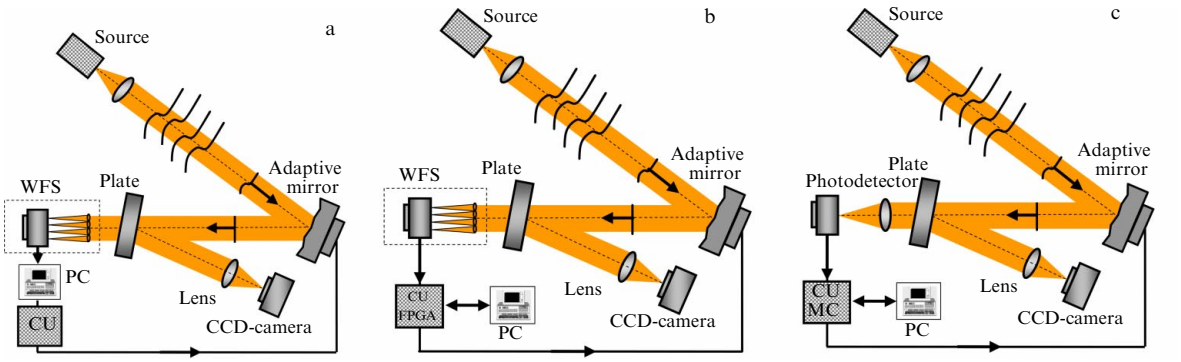

Figure 16. Scheme of adaptive optical system with the WFS control (a, b) and optimization control (c).

balanced if the Strehl ratio reaches 0.8. The necessary condition for ensuring the operation speed of the adaptive system is the high frequency of the mirror's first mechanical resonance [187].

Based on their response characteristics, all existing types of adaptive mirrors proposed since the 1970s and 1980s can be divided into two broad categories: mirrors with local and modal response functions. Some of these are of only historical interest due to their low sensitivity, slow response time, and low radiation resistance.

The first group, based on design features, includes segmented correctors (see, e.g., [188]), consisting of several movable mirror sections that, depending on the design, can be displaced in the direction perpendicular to the surface and tilted; membrane correctors [189, 190] with a set of control electrodes; monolithic correctors in the form of the piezoceramic block with the polished thin glass mirror bounded to it (see, for example, [191]). Correctors based on electrically controlled nematic liquid crystal transmitters [192–195] have high spatial resolution but low response speed and nonlinear response. MEMS (Micro-Electro-Mechanical Systems) mirrors are scalable arrays of parallel plate electrostatic actuators fabricated in silicon using semiconductor technology [196, 197]. They possess high spatial resolution of the control elements and are used in adaptive optics for astronomy and other applications (see, e.g., [198–200]), but have limited flexure of the reflecting surface, relatively small apertures, and low radiation resistance that makes it impossible to control high-power laser beams. Plates with the local drive response function [201–203] play a special role in the field of high-power lasers. They consist of the reflective optical substrate and the support, between which control piezoelectric actuators (pushers) are positioned. The action of the latter is directed perpendicular to the substrate surface. The amplitude of surface displacement in such mirrors is determined not only by the dynamic range of the actuator, but also by the elastic properties of the reflective substrate, its thickness, and the distance between the actuators. The increase of response speed of these mirrors is due to the use of special piezoceramic packages as actuators [204, 205]. Such piezo packages allow for significant mirror surface displacements ($\sim$ 10 μm and more) while maintaining high response speed (first mechanical resonance frequency of several kilohertz) [206–208]. The shape of the response functions of such mirror with stacked piezo actuators is well approximated by the Gaussian distribution [209]. Since the majority (over 90%) of the surface deformation of such mirrors occurs in the area where the actuator is located, this justifies classifying them as the mirrors with local response function. One of the drawbacks of using piezoelectric drives is the presence of hysteresis at the level of 10–15% [210]. Common drawback of mirrors with the local response function is the need for a large number of control elements to compensate for lower-order wavefront aberrations.

The second group of mirrors, which have the modal response function, includes film mirrors [211, 212], plates with actuators arranged parallel to the reflective surface [213, 214], and mirrors based on the bimorph piezoelectric element [215–217]. In the latter case, the corrector consists of the glass substrate with the piezo disc glued to it and featuring the single common electrode on the substrate side and a number of control electrodes of various configurations on the opposite side. By selecting the sufficiently large number of control electrodes and varying their positions on the surface of the piezo plate, it is possible to reproduce a large number of wavefront aberrations, including typical atmospheric ones [218–220]. One of the main advantages of such mirrors is the large range of surface displacement. In addition, technologies for creating wafer-based mirror cooling structures allow for the fabrication of cooled bimorph mirrors [221, 222]. Such mirrors can be used for the correction and shaping of high-power laser radiation parameters.

The distorted laser beam shown in Fig. 16a is reflected by an adaptive mirror, and the small portion of it passes through the splitter plate to the wavefront sensor (WFS) — the device that records information about the phase surface (wavefront). There are several known types of WFSs (including an interferometric sensor [223], the curvature sensor [224], and the pyramidal sensor [225, 226]), however, the Shack–Hartmann WFS [227, 228] shown in Fig. 16a is the most widely used in laser adaptive optics due to its simplicity and reliability. In the Shack–Hartmann WFS, the radiation passes through an array of microlenses, the plane of which is optically conjugate to the plane of the adaptive mirror. This WFS can also serve as a tool for determining turbulence parameters [229–235]. The information from the WFS is processed by the computer to determine local phase gradients, which can be used to reconstruct the wavefront using the basis of mirror's response functions or Zernike polynomials [12]. The computer code then calculates the control signals (voltages) to be applied to the actuators of the adaptive mirror so that its surface corresponds as closely as possible to the phase surface. Therefore, after reflection from the deformed mirror, the beam should acquire the wavefront that is close to flat one. In addition to phase correction of the powerful laser beam, the adaptive system can solve the

problem of focusing it through an optically inhomogeneous medium in phase-conjugate mode with respect to a reference beam. Here, the adaptive system operates similarly to the system of PC at SBS, with the difference that only the phase is adjusted. However, in many practical cases, phase inhomogeneities play the decisive role in the formation of the focal spot compared to amplitude inhomogeneities.

4.2.1 Adaptive optics for CW lasers. Controlling the phase tip-tilts and the shape of the phase front of high-power lasers typically involves the use of mirrors equipped with bimorph or pusher-type piezoelectric actuators.

In the aforementioned Nd:YAG solid-state laser system [166], consisting of 7 amplifying channels with coherent summing, the power of over 100 kW was demonstrated for more than 5 minutes. The divergence of the output radiation was 2.9 diffraction limits. In each channel, wavefront flattening is performed using the deformable mirror with the WFS, followed by phase combining. The power of the amplification channel is increased until wavefront distortions are compensated. This is followed by scaling across the number of channels.

An adaptive system designed for the multi-kilowatt CO_2 laser ($\lambda = 10.6$ μm) corrected higher-order aberrations and stabilized beam jitter [236]. The bimorph deformable mirror and piezo tip-tilt phase correctors were used as executive elements. An uncooled bolometric long-wavelength IR camera was used as the photodetector in the WFS. The adaptive system reduced the amplitude of higher-order aberrations of the beam by the factor of seven at the frequency of 50 Hz and stabilized beam jitter to the level of 25 μrad at the frequency of 100 Hz.

Although the surface of the deformable mirror is smooth, it can be used to correct optical vortices with the discontinuous wavefront that form in the turbulent atmosphere (see Section 3.5). Experimental recording [237] and phase correction [238] of the wavefront of the toroidal Laguerre–Gaussian mode LG_0^1 were performed in an adaptive system with the Shack–Hartmann WFS and the bimorph mirror with 5×5 actuators situated in the square geometry. The flexible mirror cannot reproduce the phase discontinuity, therefore the correction is performed in the practical sense: the toroidal beam spot in the far field is transformed into a spot with an on-axis peak that leads to significant increasing of the Strehl ratio and the resolution of the optical system [239].

The performance of the adaptive system depends on its spatial and temporal resolution. The requirement for spatial resolution follows from the condition that the coherence radius of the radiation must exceed the distance between the actuators of the adaptive mirror (or the size of the bimorph mirror actuator) when the amplitude of surface displacement is sufficient. Temporal resolution, i.e., operation speed, depends on the sum of the times of particular processes: exposure of the frame on the WFS camera, ADC, processing of WFS data up to the calculation of control voltages, DAC, amplification and application of voltages, and mirror response. The response time of the adaptive system shown in Fig. 16a is approximately of 100 Hz, largely limited by delays in the computer's operating system included in the feedback loop and difficulties in organizing parallel computations.

In the case of the high-power laser, the dynamics of optical inhomogeneities — both within the active medium itself and along the radiation propagation path — can be significant. Since the spectrum of, for example, atmospheric refractive index fluctuations reaches frequencies in the hundreds of hertz [178], the operation of the adaptive system requires the sufficiently high response speed. Fundamental estimates of the required operation speed for the adaptive system that compensates for phase aberrations in the turbulent atmosphere were presented in [240–242].

In [243], the numerical study was conducted on the dynamic phase correction of the laser beam distorted by atmospheric turbulence in the adaptive system using the Shack–Hartmann WFS. The spatial spectrum of turbulent phase distortions corresponded to the Kolmogorov model with wind temporal displacement. It is shown that phase correction is highly effective when the operating frequency ν_{AOS} is approximately 20 times greater than the bandwidth of turbulent phase fluctuations ν_{turb}. The latter is the characteristic frequency within which the overwhelming majority ($\sim 95\%$) of the spectral 'energy' of local phase fluctuations in the laser beam is contained. The value of ν_{turb} can be quickly estimated with the help of the Shack–Hartmann WFS from the spectrum of focal spot oscillations in the WFS subaperture when its size s is close to the coherence radius r_0 (30). The results in [243] indicate that the required operating frequency of the adaptive system should be in the range of several kilohertz.

The transition to real-time adaptive optics requires, above all, high-speed computing hardware. One type of such hardware consists of systems based on the field-programmable gate array (FPGA), which is the version of the programmable logic integrated circuit (PLIC) [244, 245]. This approach provides high throughput and low computational latency, enabling high performance. The scheme of such an adaptive system is shown in Fig. 16b, where system control is built around the FPGA. The computer running the operating system is removed from the feedback loop and serves to turn the system on/off and to modify the program 'hard-coded' into the FPGA. Another type is the use of graphics processing unit (GPU) [246, 247]. Although the FPGA provide higher processing speed, the specificity of the hardware and the labor-intensive nature of software modification make this option difficult to widely implement. The more accessible approach is the use of open-source GPU software on the real-time computer.

The integration of the FPGA, as the main control element for the system as a whole, into the adaptive system with the piezoelectric adaptive mirror and Shack–Hartmann WFS with the standard CMOS camera enabled to reach the operating frequency of 2.25 kHz in the closed-loop configuration [248, 249], i.e., to actually increase the operation speed by an order of magnitude. At LULI (France), the operation speed of 1.3 kHz for the adaptive system was demonstrated using the GPU [250].

The radical increase in operation speed made it possible to study the phase correction of laser radiation beam distorted by the turbulent air flow under the wide range of the adaptive system's operating frequencies [249, 251]. The spatio-temporal phase spectrum of the distorted laser beam corresponded to the turbulence of character close to Kolmogorov law. The coherence radius of the radiation (30) implied satisfactory spatial resolution of the adaptive system. The turbulence bandwidth ν_{turb} in the experiments was lying in the range of 30–70 Hz. The experiments showed that switching to the frequency of 2 kHz allows for significant compensation of the negative influence of the atmosphere (see Fig. 17), which is consistent with the calculations [243].

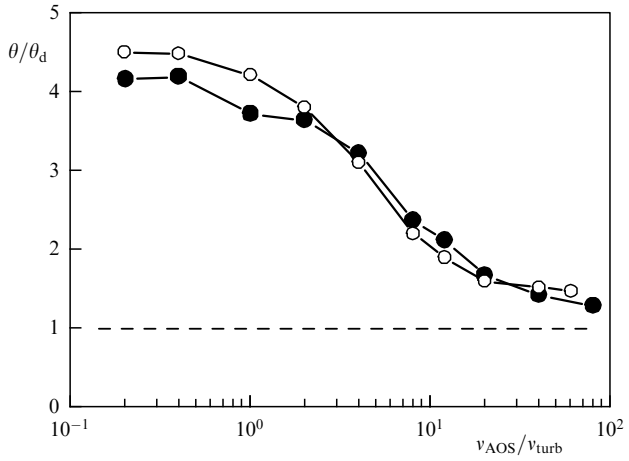

Figure 17. The laser beam divergence against adaptive correction frequency ν_{AOS} in the experiment (filled markers) and calculation (open markers).

In the adaptive system, iterative optimization control can be implemented in place of WFS control (see Section 4.1), replacing the WFS with the single-element metric sensor (see Fig. 16c). The computer is removed from the feedback loop, and the high-speed microcontroller, in which the control program is 'hard-coded,' is integrated into the control unit. Control of the adaptive system without the WFS based on the SPG algorithm has been actively studied in [172, 252–255]. As noted in Section 4.1, this approach allows not only for correcting the wavefront at the laser output but also for focusing the beam through the optically inhomogeneous medium in the feedback loop during remote optical monitoring of the irradiation spot [167, 256, 257].

The SPG algorithm is widely used to control adaptive mirrors [258–261]. The microcontroller can operate at frequencies up to 55 MHz. This is significantly lower than the clock speeds of modern computer processors, but commands are processed in real time without the operating system delays that significantly increases operating speed. The single-element photodetector (photodiode or photomultiplier) also allows for high-frequency operation, unlike the multi-element CCD or CMOS cameras shown in Fig. 16a, b. The closed-loop operating frequency of the adaptive system achieved in experiments [258], 3–5 kHz under optimal algorithm parameters, was limited by the inertia of the bimorph mirror.

It is worth noting one advantage of using the SPG control compared to the WFS [262]. The WFS operates with the beam characterized by the single wavefront, i.e., the beam generated by a certain effective homocentric source. However, in some cases, such as in the multimode laser generator, the beam consists of many independent spatial modes, each characterized by its own wavefront. As a result, the WFS measures the certain average wavefront of the beam, which may generally turn out to be 'close to flat,' while the beam has high divergence. SPG control is capable of reducing the divergence of multimode radiation with minimal loss of output power. In the iterative SPG process, the algorithm 'selects' the mode that initially makes the greatest contribution to the metric and adjusts the adaptive mirror to it.

Significant improvement in the performance of adaptive optics using the WFS [249] and the implementation of the SPG control algorithm have made it possible to conduct even some astronomical observations using the laser adaptive system [263]. It is worth noting that specialized adaptive optics for astronomical applications (see reviews [264–268]) also involves the use of hardware-based control of adaptive systems. MEMS mirrors and special cameras in the Shack–Hartmann WFS with the subaperture in the form of the quadrant photodetector contribute to the operation speed of several kHz, whereas in [263] the laser adaptive system used piezoelectric mirrors and CMOS camera in the WFS. The Rayleigh laser guide star, which was activated at the altitude of 3–6 km, served as the reference source; the source was strobed using the acousto-optic filter. Increased operation speed is accompanied by the decrease in signal accumulation time on the WFS, so under conditions of low signal-to-noise ratio the detection scheme is supplemented by an electro-optical converter. It placed between the acousto-optic filter and the WFS to amplify the received signal. The incorporation of electro-optical converter is particularly relevant when weather conditions deteriorate and the formation distance of the laser guide star increases. Fast WFS control compensating for the influence of the ground atmospheric layer was combined with slower SPG control used for automatic focusing under conditions of the extended reference source. As a result, the reduction in the apparent size of the natural bright stars from 3–5″ to 0.3″ was demonstrated (see Fig. 18). The Strehl ratio exceeded 0.1 at $r_0 = 6$ cm, in agreement with the calculation results.

4.2.2 Adaptive optics for pulsed lasers. Today, the high-power pulsed lasers with pulse durations in the nanosecond range are being developed to study the interaction of high energy density radiation with matter and to initiate inertial controlled fusion reaction (for example, the largest facilities in the United States [269], France [270], Russia [271, 272], and China [273] using neodymium phosphate glass pumped by pulsed xenon lamps). These facilities allow energy levels of several megajoules to be achieved through the incoherent combining of radiation from many (up to 192) independent laser channels. Adaptive systems in each channel are an integral part of the facilities and are designed to measure and correct wavefront distortions of the laser beam in order to increase its intensity and uniformity under focusing [274–280]. The specific features of adaptive correction here are the pulsed nature of the radiation and large (up to 400 mm and larger) beam apertures, which require large-scale adaptive optics with many dozens of control elements. The adaptive mirror is located in the multi-pass amplification path, usually in place of one of the end mirrors. Adaptive systems employ flexible mirrors with piezoelectric or mechanical actuators driven by precision stepper motors [281], and typically use the Shack–Hartmann WFS. Turbulent dynamic phase distortions are minimized, and the beam propagates through the tube for most of the path.

The large-scale phase aberrations of the output laser beam after several passes through the amplification path consist of two components: static aberrations caused by manufacturing inaccuracies in the optical elements and their positioning, and thermal aberrations arising in the active elements of the amplifiers due to their heating during pumping [282]. Although thermal aberrations are dynamic, the change in the thermally induced refractive index is insignificant during the pulse duration. Adaptive phase correction is effectively performed in the static mode: the wavefront is measured integrally over the pulse, and the adaptive mirror is preset

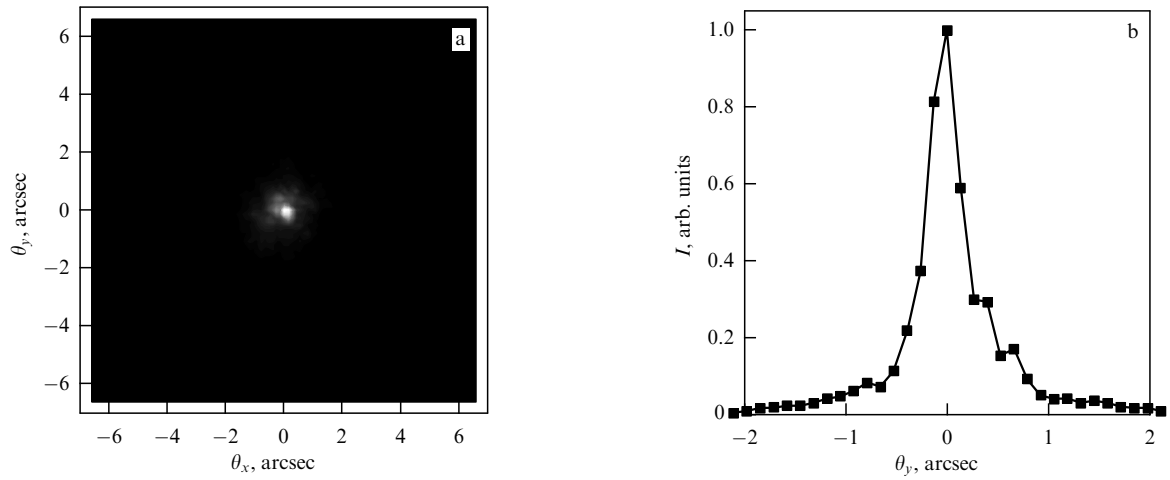

Figure 18. Short-exposure image of Vega star under switching-on the adaptive correction (a) and its section (b).

before the next laser pulse. The schematic diagram of the adaptive system shown in Fig. 16a is used. In practice, a large number of technical problems must be solved, related to determining the reference Hartmannogram, improving the measurement accuracy of both types of aberrations, the influence of optical inhomogeneities in the diagnostic channels, etc.

The surface of the adaptive mirror is initially shaped so that after passing through the amplification path, the wavefront of an alignment beam at the output is as close to flat as possible. To conserve the dynamic range of the applied voltages, this can be achieved by manually adjusting the position of the mirror actuators. Further correction of the wavefront is performed by applying voltages to the piezo actuators. Applying the voltages obtained during the correction of static aberrations, an experiment is conducted under pumping the amplifiers, and the wavefront is measured. The thermal aberration pattern is determined by subtracting the residual wavefront after static aberration correction from the resulting wavefront. The largest contribution to the pattern of large-scale aberrations is made by Zernike polynomials up to the 8th order [283]. Using adaptive phase correction, it is possible to reduce the phase RMS deviation to the level of less than $\lambda/5$ (see, for example, [284]).

Adaptive optics has been successfully applied in the PHELIX laser systems (Germany) [285] and in several LULI (France) lasers [286], which can operate both in nanosecond pulse mode with energies up to 1 kJ, used primarily for plasma heating, and in high-power subpicosecond pulse mode.

Significant progress is currently being made in the development of solid-state laser systems with femtosecond pulse durations and ultra-high peak power, creating unique conditions for fundamental research of their interaction with matter. The main sources of wavefront distortion in such lasers are aberrations in wide-aperture optical elements in the amplification path used for beam expansion and rotation as well as for pulse compression. In addition, the focusing parabolic mirror in the interaction chamber also introduces significant distortions. As the energy increases, thermal deformations of the active elements during laser amplification begin to manifest (in the case of parametric amplification this problem is less acute). All these circumstances require the use of adaptive optics [287]. Adaptive systems with bimorph mirrors and Shack–Hartmann WFS for ultrashort-pulse ultrahigh-power lasers have been successfully used on the 10-TW Ti:Sa ATLAS facility (Germany) [288], on the 100-TW facility with the pulse repetition rate of 10 Hz (Japan, JAERI), where the Strehl ratio of 0.8 and the peak intensity on the target of over 10^{20} W cm^{-2} were achieved [289], and on the 100-TW facility (Canada) [290].

Currently, many modern femtosecond laser systems have already reached and exceeded the petawatt power level [291–295]. The intensity of focused laser radiation with ultrashort pulses is generally in the range of $10^{19}-10^{21}$ W cm^{-2}, which is sufficient for conducting relativistic experiments on the acceleration of electrons and ions, the generation of X-rays and gamma rays, etc. However, to study extreme phenomena in quantum electrodynamics, up to approaching the Schwinger limit, the intensity must be significantly higher than 10^{22} W cm^{-2} [296]. Increasing the intensity to this level and beyond is currently possible by shortening the pulse [297], transitioning to the multi-petawatt level including through the construction of multi-channel systems [298–300] with adaptive optics [301, 302]. The implementation of the wide-aperture adaptive system with the 320-mm-diameter bimorph mirror with 127 control electrodes [303] in the Ti:Sa laser has already made it possible to achieve the peak intensity of 10^{23} W cm^{-2} at the power of 4.2 PW [304].

Further development in this area involves increasing the aperture of the adaptive mirrors, refining the design of the actuators, and improving the technical approaches to controlling the adaptive optics. For the petawatt-level, picosecond-duration LFEX facility [305], the deformable mirror with aperture 410×468 mm was developed, controlled by bimorph piezo plates and multilayer piezo actuators. Investigation of the mirror using the Fizeau interferometer and the WFS revealed that surface flatness was improved to as low as 0.033 μm RMS [306]. Despite the static nature of adaptive system operation in such lasers, increasing attention has recently been paid to the possibility of accounting for dynamic phase aberrations of various time scales. On the Ti:Sa Apollon facility (France), the use of real-time adaptive optics with the pilot beam allowed for continuous control of the wavefront and increased the Strehl ratio of the statically corrected beam from 0.62 to 0.96 [250]. On the PEARLE facility (Russia) with parametric amplification, an increase in peak radiation intensity of nearly an order of magnitude during focusing was demonstrated when using the dynamic

method for determining the reference wavefront in the WFS, based on the processing of synchronously acquired data on the near and far fields [307–309]. This allows for the correction of, among other things, phase distortions arising from the nonlinear post-compression of the laser pulse.

5. Conclusions

Ideas about the possibility of controlling the radiation using linear adaptive optics for astronomical observations were first proposed in the 1950s. Beyond astronomy, the concept of adaptive optics has proven fruitful in materials science, medicine, electronics, biology, and quantum electronics with the advent of lasers in the 1960s. Achieving the small angular divergence of radiation is one of the most important challenges in laser design. This is especially relevant for high-power lasers, whose optical path and active medium typically contain significant static and dynamic optical inhomogeneities, significantly degrading the beam quality. When considering the problem more broadly, it is necessary to consider optical inhomogeneities along the radiation propagation path.

Adaptive optics currently plays a key role in solving the angular divergence problem. The use of nonlinear methods, particularly phase conjugation at SBS, allows the high-power lasers with pulse durations of ~ 0.01 μs–1 ms to achieve divergence close to the diffraction limit. Virtually no high-power solid-state laser in the nano- and femtosecond range operates without adaptive beam control using the flexible mirrors. High-power continuous-wave gas and solid-state lasers, which have recently made technological advances thanks to the use of diode pumping, are also unimaginable without adaptive optics. Adaptive phase control plays the key role in the creation of multichannel fiber-optics laser systems with coherent beam combining. Further development of adaptive optics technologies is associated with the search for new media, increased performance, and the correction of phase distortions in turbulent atmosphere, including the use of optimization schemes. The creation of multichannel femtosecond systems will require solving the problem of spatiotemporal super-looking and beam super-localization, which presents a new challenge for adaptive control of laser radiation.

This work was partially supported by the scientific program of the National Center for Physics and Mathematics of RF, Section 4, stage 2023–2025.

References

1. Dmitriev V G *Nelineinaya Optika i Obrashchenie Volnovogo Fronta* (Nonlinear Optics and Phase Conjugation) (Moscow: Fizmatlit, 2003)
2. Garmire E *New J. Phys.* **19** 011003 (2017)
3. Wolff C et al. *J. Opt. Soc. Am. B* **38** 1243 (2021)
4. Wang Y, Zhang M *Sensors* **22** 6062 (2022)
5. Merklein M et al. *Appl. Phys. Rev.* **9** 041306 (2022)
6. Zeldovich B Ya et al. *JETP Lett.* **15** 109 (1972); *Pis'ma Zh. Eksp. Teor. Fiz.* **15** 160 (1972)
7. Zel'dovich B Ya, Pilipetsky N F, Shkunov V V *Obrashchenie Volnovogo Fronta* (Moscow: Nauka, 1985); Translated into English: *Principles of Phase Conjugation* (Berlin: Springer-Verlag, 1985)
8. Bespalov V I, Pasmanik G A *Nelineinaya Optika i Adaptivnye Lazernye Sistemy* (Moscow: Nauka, 1986); Translated into English: *Nonlinear Optics and Adaptive Laser Systems* (Commack, NY: Nova Sci. Publ., 1994)
9. Ragul'skii V V *Obrashchenie Volnovogo Fronta pri Vynuzhdennom Rasseyanii Sveta* (Phase Conjugation in Stimulated Light Scattering) (Moscow: Nauka, 1990)
10. Babcock H W *Publ. Astron. Soc. Pacif.* **65** 229 (1953)
11. Linnik V P *Opt. Spektrosk.* **25** 401 (1957)
12. Vorontsov M A, Shmal'gauzen V I *Printsipy Adaptivnoi Optiki* (Principles of Adaptive Optics) (Moscow: Nauka, 1985)
13. Lukin V P *Atmosfernaya Adaptivnaya Optika* (Novosibirsk: Nauka, 1986); Translated into English: *Atmospheric Adaptive Optics* (Bellingham, Wash.: SPIE, 1995)
14. Hardy J W *Adaptive Optics for Astronomical Telescopes* (New York: Oxford Univ. Press, 1998)
15. Tyson R K *Principles of Adaptive Optics* (Boston: Academic Press, 1998)
16. Burns S A et al. *Prog. Retinal Eye Res.* **68** 1 (2019)
17. Tyson R K *Appl. Opt.* **35** 3640 (1996)
18. Kubby J A *Adaptive Optics for Biological Imaging* (Boca Raton, FL: Taylor and Francis, 2013)
19. Kudryashov A, Weber H *Laser Resonators: Novel Design and Development* (Bellingham, WA: SPIE Press, 1999)
20. Pantell R H, Puthoff H E *Osnovy Kvantovoi Elektroniki* (Moscow: Mir, 1972); Translated from English: *Fundamentals of Quantum Electronics* (New York: Wiley, 1969)
21. Khanin Ya I *Kvantovaya Radiofizika* (Quantum Radiophysics) Vol. 2 *Dinamika Kvantovykh Generatorov* (Dynamics of Quantum Oscillators) (Moscow: Sovetskoe Radio, 1975)
22. Allen L, Eberly J H *Opticheskii Rezonans i Dvukhurovnevye Atomy* (Moscow: Mir, 1978); Translated from English: *Optical Resonance and Two-Level Atoms* (New York: Wiley, 1975)
23. Leontovich M *Izv. Akad. Nauk. SSSR, Ser. Fiz.* **8** (1) 16 (1944)
24. Scully M O, Zubairy M S *Kvantovaya Optika* (Moscow: Fizmatlit, 2003); Translated from English: *Quantum Optics* (Cambridge: Cambridge Univ. Press, 1997)
25. Hopf F A, Meystre P, McLaughlin D W *Phys. Rev. A* **13** 777 (1976)
26. Kryukov P G, Letokhov V S *Sov. Phys. Usp.* **12** 641 (1970); *Usp. Fiz. Nauk* **99** 169 (1969)
27. Starikov F A et al. *Proc. SPIE* **5197** 60 (2003)
28. Starikov F A et al. *Quantum Electron.* **39** 825 (2009); *Kvantovaya Elektron.* **39** 825 (2009)
29. Gasparyan P D, Starikov F A, Starostin A N *Phys. Usp.* **41** 761 (1998); *Usp. Fiz. Nauk* **168** 843 (1998)
30. Bethe H A, Salpeter E E *Kvantovaya Mekhanika Atomov s Odnim i Dvumya Elektronami* (Moscow: GIFML, 1960); Translated from English: *Quantum Mechanics of One- and Two- Electron Atoms* (Berlin: Springer, 1957)
31. Starunov V S, Fabelinskii I L *Sov. Phys. Usp.* **13** 428 (1970); *Usp. Fiz. Nauk* **98** 441 (1969)
32. Starikov F A et al., in *Proc. of the Intern. Conf. on LASERS'99* (Eds V J Corcoran, T A Corcoran) (McLean, VA: STS Press, 2000) p. 482
33. Starikov F A et al. *Proc. SPIE* **3930** 12 (2000)
34. Bogachev V A, Kochemasov G G, Starikov F A *Quantum Electron.* **38** 849 (2008); *Kvantovaya Elektron.* **38** 849 (2008)
35. Bogachev V A, Maslov N V, Starikov F A *Quantum Electron.* **40** 341 (2010); *Kvantovaya Elektron.* **40** 341 (2010)
36. Raymer M G, Mostowski J *Phys. Rev. A* **24** 1980 (1981)
37. Raymer M G et al. *Phys. Rev. A* **32** 332 (1985)
38. Vuks M F *Rasseyanie Sveta v Gazakh, Zhidkostyakh i Rastvorakh* (Scattering of Light in Gases, Liquids and Solutions) (Leningrad: Izd. Leningrad. Univ., 1977)
39. Afshaarvahid S, Munch J *J. Nonlin. Opt. Phys. Mater.* **10** (1) 1 (2001)
40. Akinyimika Adewale et al. *High Power Laser Part. Beams* **33** 111007 (2021) DOI:10.11884/HPLPB202133.210313
41. Brederlow G, Fill E, Witte K J *Moshchnyi Iodnyi Lazer* (Moscow: Energoatomizdat, 1985); Translated from English: *The High-Power Iodine Laser* (Heidelberg: Springer, 1983)
42. Kasper J V V, Pimentel G C *Appl. Phys. Lett.* **5** 231 (1964)
43. Arzhanov V P et al. *Sov. J. Quantum Electron.* **22** 118 (1992); *Kvantovaya Elektron.* **19** 135 (1992)
44. Anan'ev Yu A *Sov. Phys. Usp.* **14** 197 (1971); *Usp. Fiz. Nauk* **103** 705 (1971)
45. Anan'ev Yu A *Opticheskie Rezonatory i Problema Raskhodimosti Lazernogo Izlucheniya* (Optical Resonators and the Problem of Laser Beam Divergence) (Moscow: Nauka, 1979)
46. Belousova I M et al. *Sov. Phys. JETP* **31** 791 (1970); *Zh. Eksp. Teor. Fiz.* **58** 1481 (1970)

47. Golubev L E et al., in *Kvantovaya Elektronika* (Quantum Electronics) Iss. 6(18) (Ed. N G Basov) (Moscow: Sovetskoe Radio, 1973) p. 23
48. Zaretskii A I et al. *Sov. J. Quantum Electron.* **4** 649 (1974); *Kvantovaya Elektron.* **1** 1185 (1974)
49. Zykov L I et al. *Sov. Phys. JETP* **40** 447 (1975); *Zh. Eksp. Teor. Fiz.* **67** 902 (1974)
50. Zykov L I et al. *Sov. J. Quantum Electron.* **5** 71 (1975); *Kvantovaya Elektron.* **2** 123 (1975)
51. Danilov O B, Novoselov N A, Spiridonov V V *Opt. Spectrosc.* **39** 382 (1975); *Opt. Spektrosk.* **39** 680 (1975)
52. Borovich B L et al. *Sov. J. Quantum Electron.* **5** 695 (1975); *Kvantovaya Elektron.* **2** 1282 (1975)
53. Kirillov G A et al. *Sov. J. Quantum Electron.* **7** 357 (1977); *Kvantovaya Elektron.* **4** 644 (1977)
54. Zaretskii A I et al. *Sov. J. Quantum Electron.* **9** 751 (1979); *Kvantovaya Elektron.* **6** 1278 (1979)
55. Alekhin B V et al. *Sov. J. Quantum Electron.* **9** 1148 (1979); *Kvantovaya Elektron.* **6** 1948 (1979)
56. Witte K J *J. Phys. D* **12** 9 (1979)
57. Alekhin B V et al. *Sov. J. Quantum Electron.* **10** 872 (1980); *Kvantovaya Elektron.* **7** 1516 (1980)
58. Baker H, King T *IEEE J. Quantum Electron.* **17** 1828 (1981)
59. Nosach O Yu, Ragul'skii V V *Opt. Spectrosc.* **85** 918 (1998); *Opt. Spektrosk.* **85** 999 (1998)
60. Nosach O Yu et al. *JETP Lett.* **16** 435 (1972); *Pis'ma Zh. Eksp. Teor. Fiz.* **16** 617 (1972)
61. Wang V, Giuliano C *IEEE J. Quantum Electron.* **13** 895 (1977)
62. Pilipetskii N F, Popovichev V I, Ragul'skii V V *JETP Lett.* **27** 585 (1978); *Pis'ma Zh. Eksp. Teor. Fiz.* **27** 619 (1978)
63. Dolgopolov Yu V et al. *Sov. Phys. JETP* **49** 458 (1979); *Zh. Eksp. Teor. Fiz.* **76** 908 (1979)
64. Bespalov V I (Exec. Ed.) *Obrashchenie Volnovogo Fronta Opticheskogo Izlucheniya v Nelineinykh Sredakh* (Optical Radiation Phase Conjugation in Nonlinear Media) (Gorky: IPF AN SSSR, 1979)
65. Bespalov V I (Exec. Ed.) *Obrashchenie Volnovogo Fronta Opticheskogo Izlucheniya v Nelineinykh Sredakh* (Optical Radiation Phase Conjugation in Nonlinear Media) (Gorky: IPF AN SSSR, 1982)
66. Fisher R A (Ed.) *Optical Phase Conjugation* (New York: Academic Press, 1983) DOI:10.1016/C2009-0-21908-8
67. Sidorovich V G *Zh. Tekh. Fiz.* **46** 2168 (1976)
68. Bel'dyugin I M et al. *Sov. J. Quantum Electron.* **6** 1349 (1976); *Kvantovaya Elektron.* **3** 2467 (1976)
69. Kochemasov G G, Nikolaev V D *Sov. J. Quantum Electron.* **7** 60 (1977); *Kvantovaya Elektron.* **4** 115 (1977)
70. Bespalov V I, Betin A A, Pasmanik G A *Radiophys. Quantum Electron.* **20** 544 (1977); *Izv. Vyssh. Ucheb. Zaved. Ser. Radiofiz.* **20** 791 (1977)
71. Zel'dovich B Ya, Shkunov V V *Sov. J. Quantum Electron.* **7** 1345 (1977); *Kvantovaya Elektron.* **4** 2353 (1977)
72. Bel'dyugin I M, Zemskov E M *Sov. J. Quantum Electron.* **8** 1163 (1978); *Kvantovaya Elektron.* **5** 2055 (1978)
73. Kochemasov G G, Nikolaev V D *Sov. J. Quantum Electron.* **9** 1155 (1979); *Kvantovaya Elektron.* **6** 1960 (1979)
74. Betin A A, Pasmanik G A *Sov. J. Quantum Electron.* **6** 1204 (1976); *Kvantovaya Elektron.* **3** 2215 (1976)
75. Blashchuk V N et al. *Sov. Tech. Phys. Lett.* **3** 83 (1977); *Pis'ma Zh. Tekh. Fiz.* **3** 211 (1977)
76. Bespalov V I, Betin A A, Pasmanik G A *Sov. Tech. Phys. Lett.* **3** 85 (1977); *Pis'ma Zh. Tekh. Fiz.* **3** 215 (1977)
77. Baranova N B, Zel'dovich B Ya, Shkunov V V *Sov. J. Quantum Electron.* **8** 559 (1978); *Kvantovaya Elektron.* **5** 973 (1978)
78. Baranova N B, Zel'dovich B Ya *Sov. J. Quantum Electron.* **10** 555 (1980); *Kvantovaya Elektron.* **7** 973 (1980)
79. Dolgopolov Yu V et al. *Zh. Tekh. Fiz.* **51** 1764 (1981)
80. Heuer A, Menzel R, in *Phase Conjugate Laser Optics* (Eds A Brignon, J-P Huignard) (New York: John Wiley and Sons, 2004) p. 19, DOI:10.1002/0471728446.ch2
81. Suni P, Falk J *J. Opt. Soc. Am. B* **3** 1681 (1986)
82. Miller E J, Skeldon M D, Boyd R W *Appl. Opt.* **28** 92 (1989)
83. Kir'yanov Yu F et al. *Sov. J. Quantum Electron.* **21** 533 (1991); *Kvantovaya Elektron.* **18** 588 (1991)
84. Kir'yanov Yu F et al. *Sov. J. Quantum Electron.* **22** 634 (1992); *Kvantovaya Elektron.* **19** 684 (1992)
85. Kir'yanov Yu F et al. *Quantum Electron.* **29** 970 (1999); *Kvantovaya Elektron.* **29** 132 (1999)
86. Lehmberg R H *Opt. Commun.* **43** 369 (1982)
87. Lehmberg R H *J. Opt. Soc. Am.* **73** 558 (1983)
88. Anikeev I Yu, Zubarev I G, Mikhailov S I *Sov. J. Quantum Electron* **16** 88 (1986); *Kvantovaya Elektron.* **13** 142 (1986)
89. Hu P H, Goldstone J A, Ma S S *J. Opt. Soc. Am. B* **6** 1813 (1989)
90. Kir'yanov Yu F et al. *Sov. J. Quantum Electron* **21** 1341 (1991); *Kvantovaya Elektron.* **18** 1454 (1991)
91. Kummrow A *Opt. Commun.* **96** 185 (1993)
92. Moore T R, Boyd R W *J. Non. Opt. Phys. Mater.* **5** 387 (1996)
93. Moore T R, Fischer G L, Boyd R W *J. Mod. Opt.* **45** 735 (1998)
94. Vlad V I, Babin V, Mocofanescu A *J. Optoelectron. Adv. Mater.* **4** 581 (2002)
95. Mak A A et al. *Lazery na Neodimovom Stekle* (Moscow: Nauka, 1990)
96. Valley G *IEEE J. Quantum Electron.* **22** 704 (1986)
97. Gaeta A L, Boyd R W *Phys. Rev. A* **44** 3205 (1991)
98. Damzen M, Hutchinson H *IEEE J. Quantum Electron.* **19** 7 (1983)
99. Dianov E M et al. *Opt. Quantum Electron.* **21** 381 (1989)
100. Boyd R W, Rzaewski K, Narum P *Phys. Rev. A* **42** 5514 (1990)
101. Chu P, Kanefsky M, Falk J *J. Appl. Phys.* **71** 4653 (1992)
102. Afshaarvahid S, Devrelis V, Munch J *Phys. Rev. A* **57** 3961 (1998)
103. Bobrov S T et al. *Opt. Spektrosk.* **62** 402 (1987)
104. Gratsianov K V et al. *Opt. Spektrosk.* **68** 617 (1990)
105. Bobrov S T, Greisukh G I, Turkevich Yu G *Optika Difraktsionnykh Elementov i Sistem* (Optics of Diffractive Elements and Systems) (Leningrad: Mashinostroenie, 1986)
106. Kulikov S M et al. *Proc. SPIE* **1628** 90 (1992)
107. Dolgopolov Yu V et al. *Proc. SPIE* **1980** 23 (1992)
108. Dolgopolov Yu V et al. *Izv. Akad. Nauk SSSR, Ser. Fiz.* **58** 35 (1994)
109. Kochemasov G G, Starikov F A *Opt. Commun.* **17** 161 (1999)
110. Dolgopolov Yu V et al., in *Proc. of the Intern. Conf. on LASERS'99* (Eds V J Corcoran, T A Corcoran) (McLean, VA: STS Press, 2000) p. 466
111. Starikov F A et al. *Proc. SPIE* **4353** 202 (2001)
112. Starikov F A et al. *Izv. Ross. Akad. Nauk. Ser. Fiz.* **65** 935 (2001)
113. Dolgopolov Yu et al., in *Technical Digest of CLEO/Europe 2003* (Europhysics Conf. Abstracts, Vol. 27E) Paper CF5-4-FRI
114. Starikov F, Kochemasov G, in *Adaptive Optics for Industry and Medicine. Proc. of the 4th Intern. Workshop, Munster, Germany, Oct. 19–24, 2003* (Springer Proc. in Physics, Vol. 102, Ed. U Wittrock) (Berlin: Springer, 2005) p. 291, DOI:10.1007/3-540-28867-8_30
115. Bogachev V A et al. *Quantum Electron.* **42** 531 (2012); *Kvantovaya Elektron.* **42** 531 (2012)
116. Eroshenko V A et al. *Voprosy Atom. Nauki Tekh. Ser. Teor. Priklad. Fiz.* (3) 25 (1990)
117. Starikov F A et al. *Proc. SPIE* **5147** 60 (2003)
118. Starikov F A et al. *Proc. SPIE* **5479** 81 (2004)
119. Kulikov S M et al. *Laser Part. Beams* **17** 765 (1999)
120. Kong H J et al. *Opt. Rev.* **4** 277 (1997)
121. Omatsu T et al. *Laser Part. Beams* **30** 117 (2012)
122. Garanin S G et al. *Quantum Electron.* **52** 289 (2022); *Kvantovaya Elektron.* **52** 289 (2022)
123. Bogachev V A, Nemtseva A V, Starikov F A *Tech. Phys.* **69** 769 (2024); *Zh. Tekh. Fiz.* **94** 827 (2024)
124. Oraevskii A N *Trudy Fiz. Inst. Akad. Nauk SSSR* **187** 3 (1988)
125. Starikov F A, Kochemasov G G *Opt. Commun.* **193** 207 (2001)
126. Starikov F A, Kochemasov G G *Proc. SPIE* **4403** 217 (2001)
127. Starikov F A, in *Nelineinye Volny 2006* (Nonlinear Waves 2006) (Eds A V Gaponov-Grekhov, V I Nekorkin) (Nizhny Novgorod: IPF RAN, 2007) p. 206
128. Starikov F A et al. *Proc. SPIE* **7009** 70090E (2008)
129. Kopalkin A V et al. *Quantum Electron.* **41** 1023 (2011); *Kvantovaya Elektron.* **41** 1023 (2011)
130. Aksenov V P et al. *Proc. SPIE* **5894** 5894O7 (2005)
131. Atuchin V V et al. *Proc. SPIE* **6054** 188 (2006)
132. Bagdasarov V Kh et al. *Quantum Electron.* **39** 785 (2009); *Kvantovaya Elektron.* **39** 785 (2009)
133. Fan T Y *IEEE J. Sel. Top. Quantum Electron.* **11** 567 (2005)

134. Bruesselbach H et al. *J. Opt. Soc. Am. B* **22** 347 (2005)
135. Augst S J et al. *Optics Lett.* **29** 474 (2004)
136. Pyrkov Yu N, Trikshev A I, Tsvetkov V B *Quantum Electron.* **42** 790 (2012); *Kvantovaya Elektron.* **42** 790 (2012)
137. Bellanger C et al. *Opt. Lett.* **33** 2937 (2008)
138. Peng W et al. *Micromachines* **12** 1426 (2021)
139. Brauch U et al. *Appl. Phys. B* **128** 58 (2022)
140. Rastogi V, Chaurasia S *Photonics* **11** 942 (2024)
141. Kurkov A S, Dianov E M *Quantum Electron.* **34** 881 (2004); *Kvantovaya Elektron.* **34** 881 (2004)
142. Zhou P et al. *Sci. China Technol. Sci.* **60** 1784 (2017)
143. Zervas M N, Codemard C A *IEEE J. Select. Top. Quantum Electron.* **20** 219 (2014)
144. Dawson J W et al. *Opt. Express* **16** 13240 (2008)
145. Zhu J et al. *Opt. Express* **19** 18645 (2011)
146. Shi W et al. *Appl. Opt.* **53** 6554 (2014)
147. Huang B, Wang J, Shao X *Photonics* **10** 282 (2023)
148. Huang R K et al. *IEEE Photon. Technol. Lett.* **19** 209 (2007)
149. Wirth C et al. *Opt. Express* **17** 1178 (2009)
150. Schmidt O et al. *Opt. Lett.* **34** 1567 (2009)
151. Kovalev V I, Harrison R G *Opt. Lett.* **30** 1375 (2005)
152. Grime B W, Roh W B, Alley T G *Opt. Lett.* **30** 2415 (2005)
153. Fan T Y *IEEE J. Select. Top. Quantum Electron.* **11** 567 (2005)
154. Brignon A (Ed.) *Coherent Laser Beam Combining* (New York: Wiley-VCH Verlag, 2013) DOI:10.1002/9783527652778
155. Protz R et al. *Proc. SPIE* **8547** 854708 (2013)
156. Likhanskii V V, Napartovich A P *Sov. Phys. Usp.* **33** 228 (1990); *Usp. Fiz. Nauk* **160** (3) 101 (1990)
157. Vysotsky D V, Napartovich A P *Quantum Electron.* **49** 989 (2019); *Kvantovaya Elektron.* **49** 989 (2019)
158. Anderegg J et al. *Proc. SPIE* **6102** 61020U (2006)
159. Yu C et al. *Opt. Lett.* **36** 2686 (2011)
160. Redmond S et al. *Opt. Lett.* **37** 2832 (2012)
161. Thielen P, Ho J, Burchman D *Opt. Lett.* **37** 3741 (2012)
162. Flores A et al. *Opt. Eng.* **55** 096101 (2016)
163. Yu C X et al. *Elect. Lett.* **42** 1024 (2006)
164. Kansky J E et al. *Proc. SPIE* **6306** 63060G (2006)
165. Goodno G D et al. *Opt. Lett.* **31** 1247 (2006)
166. Marmo J et al. *Proc. SPIE* **7195** 719507 (2009)
167. Vorontsov M A, Kolosov V *J. Opt. Soc. Am. A* **22** 126 (2005)
168. Vorontsov M A, Weyrauch T *Appl. Opt.* **55** 9950 (2016)
169. Cauwenberghs G, in *Advances in Neural Information Processing Systems* Vol. 5 (Eds S Hanson, J Cowan, C Giles) (San Mateo, CA: Morgan Kaufmann Publ., 1993) p. 244
170. Cauwenberghs G *Analog Integrated Circuits Signal Process.* **13** 195 (1997)
171. Vorontsov M A, Carhart G W, Ricklin J C *Opt. Lett.* **22** 907 (1997)
172. Vorontsov M A, Sivokon V P *J. Opt. Soc. Am. A* **15** 2745 (1998)
173. Bruesselbach H et al., in *Conf. on Lasers and Electro-Optics, CLEO, Baltimore, MD, USA, 22–27 May 2005* Vol. 1 (Piscataway, NJ: IEEE, 2005) p. 746, DOI:10.1109/CLEO.2005.201909
174. Weyrauch T et al. *Opt. Lett.* **36** 4455 (2011)
175. Volkov V A et al. *Quantum Electron.* **45** 1125 (2015); *Kvantovaya Elektron.* **45** 1125 (2015)
176. Fried D L *J. Opt. Soc. Am.* **56** 1380 (1966)
177. Weyrauch T et al. *Opt. Lett.* **41** 840 (2016)
178. Andrews L C, Phillips R L *Laser Beam Propagation through Random Media* 2nd ed. (Bellingham, WA: SPIE Press, 1998)
179. Volkov V A et al. *Quantum Electron.* **43** 852 (2013); *Kvantovaya Elektron.* **43** 852 (2013)
180. Volkov M V et al. *Quantum Electron.* **44** 1039 (2014); *Kvantovaya Elektron.* **44** 1039 (2014)
181. Volkov M V et al. *Quantum Electron.* **50** 694 (2020); *Kvantovaya Elektron.* **50** 694 (2020)
182. Freeman R H, Pearson J E *Appl. Opt.* **21** 580 (1982)
183. Nikolaev P V, Smirnov A V *Opt.-Mekh. Promyshl.* (11) 47 (1987)
184. Taranenko V G, Shanin O I *Adaptivnaya Optika* (Adaptive Optics) (Moscow: Radio i Svyaz', 1990)
185. Ryabova N V, Zakharenkov V F *Opt.-Mekh. Promyshl.* (6) 5 (1992)
186. Born M, Wolf E *Osnovy Optiki* (Moscow: Nauka, 1973); Translated from English: *Principles of Optics* (Oxford: Pergamon Press, 1969)
187. Harvey J E, Callahan G M *Proc. SPIE* **141** 50 (1978)
188. Sato T, Ikeda O, Ueda Y *Appl. Opt.* **17** 3945 (1978)
189. Yellin M *Proc. SPIE* **75** 97 (1976)
190. Vdovin G V, Sarro P M *Appl. Opt.* **34** 2968 (1995)
191. Feinleib J, Lipson S G, Cone P E *Appl. Phys. Lett.* **25** 311 (1974)
192. Naumov A F, in *Gologra ficheskie Metody v Nauke i Tekhnike* (Holographic Methods in Science and Technology) (Leningrad: LFTI, 1985) p. 216
193. Vasil'ev A A, Kompanets I N, Parfenov A V *Sov. J. Quantum Electron.* **13** 689 (1983); *Kvantovaya Elektron.* **10** 1079 (1983)
194. Naumov A F et al. *Opt. Lett.* **23** 992 (1998)
195. Restaino S R et al. *Opt. Express* **6** 2 (2000)
196. Bifano T G et al. *IEEE J. Select. Top. Quantum Electron.* **5** 83 (1999)
197. Bifano T *Nature Photon.* **5** 21 (2011)
198. Sun J, Xie H *Int. J. Opt.* **2011** 825629 (2011)
199. Holmström S T S, Baran U, Urey H *J. Microelectromech. Syst.* **23** 259 (2014)
200. Wang D, Watkins C, Xie H *Micromachines* **11** 456 (2020)
201. Polster H D et al. *Appl. Opt.* **8** 521 (1969)
202. Henderson W D, Sunn S V *Proc. SPIE* **179** 51 (1979)
203. Hardy J W, in *National Telecommunications Conf., New Orleans, LA, December 1–3, 1975, Conf. Record* Vol. 1 (New York: IEEE, 1975) p. 6
204. Andrianova I I et al. *Opt.-Mekh. Promyshl.* (10) 30 (1982)
205. Taranenko V G *Sov. Phys. J.* **28** 938 (1985); *Izv. Vyssh. Ucheb. Zaved. Fiz.* (11) 106 (1985)
206. Everson J H at al. *Proc. SPIE* **228** 34 (1980)
207. Freeman R H, Garcia H R *Appl. Opt.* **21** 589 (1982)
208. Albertinetti N P, Aldrich R E, Everson J H *Proc. SPIE* **179** 28 (1979)
209. Pearson J E, Hansen S *Adaptivnaya Optika* (Adaptive Optics) (Moscow: Mir, 1980); Translated from English: *J. Opt. Soc. Am.* **67** 325 (1977)
210. Garcia H R, Brooks L D *Proc. SPIE* **141** 47 (1978)
211. Sato T et al. *Appl. Opt.* **19** 1430 (1980)
212. Sato T et al. *Appl. Opt.* **20** 343 (1981)
213. Fuschetto A *Proc. SPIE* **179** 17 (1979)
214. Andronov V P, Kirchin G V, Libik L P *Opt.-Mekh. Promyshl.* (5) 17 (1982)
215. Adelman N T *Appl. Opt.* **16** 3075 (1977)
216. Kokorowski S A *J. Opt. Soc. Am.* **69** 181 (1979)
217. Steinhaus E, Lipson S G *J. Opt. Soc. Am.* **69** 478 (1979)
218. Vorontsov M A, Kudryashov A V, Shmal'gauzen V I *Sov. Phys. J.* **30** 650 (1987); *Izv. Vyssh. Ucheb. Zaved. Fiz.* (8) 11 (1987)
219. Kudryashov A V, Shmalhausen V I *Opt. Eng.* **35** 3064 (1996)
220. Cherezova T Yu, Kaptsov L N, Kudryashov A V *Appl. Opt.* **35** 2554 (1996)
221. Kudryashov A V, Samarkin V V *Opt. Commun.* **118** 317 (1995)
222. Cherezova T Yu et al. *Appl. Opt.* **40** 33 (2001)
223. Baker K L et al. *Opt. Lett.* **29** 47 (2004)
224. Craven-Bartle T V, Dorn R J, Beletic J W *Proc. SPIE* **4007** 444 (2000)
225. Ragazzoni R *J. Mod. Opt.* **43** 289 (1996)
226. Ragazzoni R et al. *Proc. SPIE* **4007** 423 (2000)
227. Hartmann J *Z. Instrumentenkunde* **24** 1 (1904); *Z. Instrumentenkunde* **24** 33 (1904); *Z. Instrumentenkunde* **24** 97 (1904)
228. Shack R B, Platt B C *J. Opt. Soc. Am.* **61** 656 (1971)
229. Fried D L *Radio Sci.* **10** 71 (1975)
230. Sarazin M, Rodier F *Astron. Astrophys.* **227** 294 (1990)
231. Tokovinin A *Publ. Astron. Soc. Pacif.* **114** 1156 (2002)
232. Antoshkin L V et al. *Opt. Atmos. Okeana* **21** 75 (2008)
233. Kovadlo P G et al. *Russ. Phys. J.* **63** 1952 (2021); *Izv. Vyssh. Ucheb. Zaved. Fiz.* **63** (11) 109 (2020)
234. Potanin S A et al. *Astrophys. Bull.* **77** 214 (2022); *Astrofiz. Byull.* **77** 241 (2022)
235. Bogachev V A et al. *JETP Lett.* **120** 573 (2024); *Pis'ma Zh. Eksp. Teor. Fiz.* **120** 598 (2024)
236. Kudryashov A et al. *Appl. Opt.* **54** 4352 (2015)
237. Starikov F A et al. *Opt. Lett.* **32** 2291 (2007)
238. Starikov F A et al. *Opt. Lett.* **34** 2264 (2009)
239. Garanin S G, Starikov F A, Malakhov Yu I, in *Adaptive Optics Progress* (Ed. R K Tyson) (Rijeka: InTech, 2013) p. 147, DOI:10.5772/53328
240. Greenwood D P *J. Opt. Soc. Am.* **67** 390 (1977)
241. Fried D L *J. Opt. Soc. Am. A* **7** 1224 (1990)

242. Karr T J *Appl. Opt.* **30** 363 (1991)
243. Volkov M V et al. *Atmos. Ocean. Opt.* **35** 250 (2022); *Opt. Atmos. Okeana* **34** 547 (2021)
244. Kudryashov A V et al. *Proc. SPIE* **10772** 250 (2018)
245. Surendran A et al. *J. Astron. Telescop. Instrum. Syst.* **4** 039001 (2018) DOI:10.1117/1.JATIS.4.3.039001
246. Truong T N et al. *Proc. SPIE* **715** 995 (2008)
247. Guyon O et al. *Proc. SPIE* **10703** 469 (2018)
248. Rukosuev A L et al. *Quantum Electron.* **50** 707 (2020); *Kvantovaya Elektron.* **50** 707 (2020)
249. Belousov V N et al. *Quantum Electron.* **51** 992 (2021); *Kvantovaya Elektron.* **51** 992 (2021)
250. Ohland J B et al. *High Power Laser Sci. Eng.* **13** e29 (2025)
251. Bogachev V A et al., in *Optika Atmosfery i Okeana. Fizika Atmosfery. XXX Mezhdunarodnyi Simpozium, Sankt-Peterburg, 01–05 Iyulya 2024* (Atmospheric and Oceanic Optics. Atmospheric Physics. XXX Intern. Symp., St. Petersburg, July 1–5, 2024) (Tomsk: Izd. IOA SO RAN, 2024) p. A255
252. Vorontsov M A et al. *J. Opt. Soc. Am. A* **13** 1456 (1996)
253. Vorontsov M A et al. *Appl. Opt.* **36** 3319 (1997)
254. Sivokon V P, Vorontsov M A *J. Opt. Soc. Am. A* **15** 234 (1998)
255. Vorontsov M A *J. Opt. Soc. Am. A* **19** 356 (2002)
256. Vorontsov M A et al. *J. Opt. Soc. Am. A* **17** 1440 (2000)
257. Weyrauch T, Vorontsov M A *Appl. Opt.* **44** 6388 (2005)
258. Garanin S G et al. *Optoelectron. Instrum. Process.* **48** 134 (2012); Translated from Russian: *Avtometriya* **48** (2) 30 (2012)
259. Garanin S et al., in *Advances in Science and Technology* Vol. 82 (Baech, Switzerland: Trans Tech Publ., 2013) p. 75, DOI:10.4028/www.scientific.net/AST.82.75
260. Garanin S G et al. *Opt. Atmos. Okeana* **26** 427 (2013)
261. Khokhlov S V et al., in *Trudy RFYaTs–VNIIEF* Iss. 19, Pt. 2 (Sarov: RFYaTs–VNIIEF, 2014) p. 380
262. Bogachev V A et al. *Atmos. Ocean. Opt.* **30** 191 (2017); *Opt. Atmos. Okeana* **29** 934 (2016)
263. Garanin S G et al. *Dokl. Ross. Akad. Nauk. Fiz. Tekh. Nauki* (2025) in press
264. Wizinowich P *Contemp. Phys.* **56** 432 (2015)
265. D'Orgeville C, Fetzer G J *Proc. SPIE* **9909** 99090R (2016) DOI:10.1117/12.2234298
266. Hippler S *J. Astron. Instrum.* **8** 1950001 (2019)
267. Guo Y et al. *Opto-Electron. Adv.* **5** 200082 (2022)
268. Rao C et al. *PhotoniX* **5** 16 (2024)
269. Miller G H, Moses E I, Wuest R C *Opt. Eng.* **43** 2841 (2004)
270. Dunne M *Nature Phys.* **2** 2 (2006)
271. Belkov S A, Garanin S G, Shagalkin Yu V, in *Proc. of the Intern. Conf. on Coherent and Nonlinear Optics and Conf. on Lasers, Applications, and Technologies, ICONO/LAT 2013, Moscow, Russia, 2013*, p. 94
272. Garanin S G et al. *Herald Russ. Acad. Sci.* **91** 250 (2021); *Vestn. Ross. Akad. Nauk* **91** 435 (2021)
273. Yang Z P et al. *Opto-Electron Eng.* **45** 180049 (2018)
274. Andre M L *Proc. SPIE* **3047** 38 (1997)
275. Wattellier B et al. *J. Opt. Soc. Am. B* **20** 1632 (2003)
276. Zacharias R A et al. *Opt. Eng.* **43** 2873 (2004)
277. Danson C N et al. *Nucl. Fusion* **44** S239 (2004)
278. Bokalo S Yu et al. *Quantum Electron.* **37** 691 (2007); *Kvantovaya Elektron.* **37** 691 (2007)
279. Zou J P et al. *Appl. Opt.* **47** 704 (2008)
280. Sueda K et al. *Plasma Phys. Fusion Technol. Laser Soc. Jpn.* **37** 45 (2009)
281. Grosset-Grange C et al. *Proc. SPIE* **6584** 658403 (2007)
282. Sutton S B et al. *Proc. SPIE* **3492** 665 (1999)
283. Belkov S A et al. *Bull. Lebedev Phys. Inst.* **51** S165 (2024); Translated from Russian: *Kvantovaya Elektron.* **53** 873 (2023)
284. Belkov S A et al. *Bull. Lebedev Phys. Inst.* **52** S377 (2025); Translated from Russian: *Kvantovaya Elektron.* **55** 1 (2025)
285. Major Z et al. *High Power Laser Sci. Eng.* **12** e39 (2024)
286. Zou J-P, Wattellier B, in *Topics in Adaptive Optics* (Ed. R Tyson) (London: InTech, 2012) p. 95, DOI:10.5772/31750
287. Druon F et al. *Opt. Lett.* **23** 1043 (1998)
288. Baumhacker H et al. *Opt. Lett.* **27** 1570 (2002)
289. Akahane Y et al. *Rev. Sci. Instrum.* **77** 023102 (2006)
290. Fourmaux S et al. *Opt. Express* **16** 11987 (2008)
291. Korzhimanov A V et al. *Phys. Usp.* **54** 9 (2011); *Usp. Fiz. Nauk* **181** 9 (2011)
292. Chu Y et al. *Opt. Lett.* **40** 5011 (2015)
293. Sung J H et al. *Opt. Lett.* **42** 2058 (2017)
294. Danson C N et al. *High Power Laser Sci. Eng.* **7** e54 (2019)
295. Li Y et al. *High Power Laser Sci. Eng.* **13** e12 (2025)
296. Di Piazza A et al. *Rev. Mod. Phys.* **84** 1177 (2012)
297. Li Z, Leng Y, Li R *Laser Photon. Rev.* 2100705 (2022)
298. Kostyukov I Yu et al. *Bull. Lebedev Phys. Inst.* **50** S635 (2023); Translated from Russian: *Kvantovaya Elektron.* **53** 95 (2023)
299. Khazanov E et al. *High Power Laser Sci. Eng.* **11** e78 (2023)
300. Chvykov V *Encyclopedia* **4** 1236 (2024)
301. Wattellier B et al. *Rev. Sci. Instrum.* **75** 5186 (2004)
302. Soloviev A A et al. *Quantum Electron.* **50** 1115 (2020); *Kvantovaya Elektron.* **50** 1115 (2020)
303. Samarkin V et al. *Appl. Sci.* **12** 1144 (2022)
304. Yoon J W et al. *Optica* **8** 630 (2021)
305. Habara H et al. *Opt. Lett.* **35** 1783 (2010)
306. Samarkin V et al. *High Power Laser Sci. Eng.* **4** e4 (2016)
307. Kotov A V et al. *Quantum Electron.* **51** 593 (2021); *Kvantovaya Elektron.* **51** 593 (2021)
308. Soloviev A et al. *Opt. Express* **30** 40584 (2022)
309. Martyanov M et al. *J. Opt. Soc. Am. B* **39** 1936 (2022)